Journal of Nanobiotechnology

RESEARCH

Open Access

MSC–microvesicles protect cartilage from degradation in early rheumatoid arthritis via immunoregulation

Shixiong Wei[1,2†], Rui-Juan Cheng[2†], Sujia Li[2†], Chenyang Lu[2], Qiuping Zhang[2], Qiuhong Wu[2], Xueting Zhao[2], Xinping Tian[1*], Xiaofeng Zeng[1*] and Yi Liu[2*]

Abstract

Objective As research into preclinical rheumatoid arthritis (pre-RA) has advanced, a growing body of evidence suggests that abnormalities in RA-affected joint cartilage precede the onset of arthritis. Thus, early prevention and treatment strategies are imperative. In this study, we aimed to explore the protective effects of mesenchymal stem cell (MSC)-derived microvesicles (MVs) on cartilage degradation in a collagen-induced arthritis (CIA) mouse model.

Methods A CIA mouse model was established to observe early pathological changes in cartilage (days 21-25) through histological and radiological examinations. On day 22, MSCs-MVs were intravenously injected into the mice with CIA. Radiological, histological, and flow cytometric examinations were conducted to observe inflammation and cartilage changes in these mice compared to the mice with CIA and the control mice. In vitro, chondrocytes were cultured with inflammatory factors such as IL-1β and TNFα to simulate inflammatory damage to cartilage. After the addition of MVs, changes in inflammatory levels and collagen expression were measured via Western blotting, immunofluorescence, enzyme-linked immunosorbent assays (ELISAs), and quantitative PCR to determine the role of MVs in maintaining chondrocytes.

Results MSC–MVs expressed vesicular membrane proteins (CD63 and Annexin V) and surface markers characteristic of MSCs (CD44, CD73, CD90, and CD105). In the early stages of CIA in mice, a notable decrease in collagen content was observed in the joint cartilage. In mice with CIA, injection of MSCs-MVs resulted in a significant reduction in the peripheral blood levels of IL-1β, TNFα, and IL-6, along with a decrease in the ratio of proinflammatory T and B cells. Additionally, MSC-MVs downregulated the expression of IL-1β, TNFα, MMP-13, and ADAMTS-5 in cartilage while maintaining the stability of type I and type II collagen. These MVs also attenuated the destruction of cartilage, which was evident on imaging. In vitro experiments demonstrated that MSC-MVs effectively suppressed the secretion of the inflammatory factors IL-1β, TNFα, and IL-6 in stimulated peripheral blood mononuclear cells (PBMCs).

Conclusions MSCs-MVs can inhibit the decomposition of the inflammation-induced cartilage matrix by regulating immune cell inflammatory factors to attenuate cartilage destruction. MSC-MVs are promising effective treatments for the early stages of RA.

†Shixiong Wei, Rui-Juan Cheng and Sujia Li contributed equally to this work.

*Correspondence:
Xinping Tian
tianxp6@126.com
Xiaofeng Zeng
zengxfpumc@163.com
Yi Liu
yiliu8999@wchscu.cn

Keywords Rheumatoid arthritis, Mesenchymal stem cells, Microvesicles, Treatment, Cartilage, Immunoregulation

Graphical Abstract

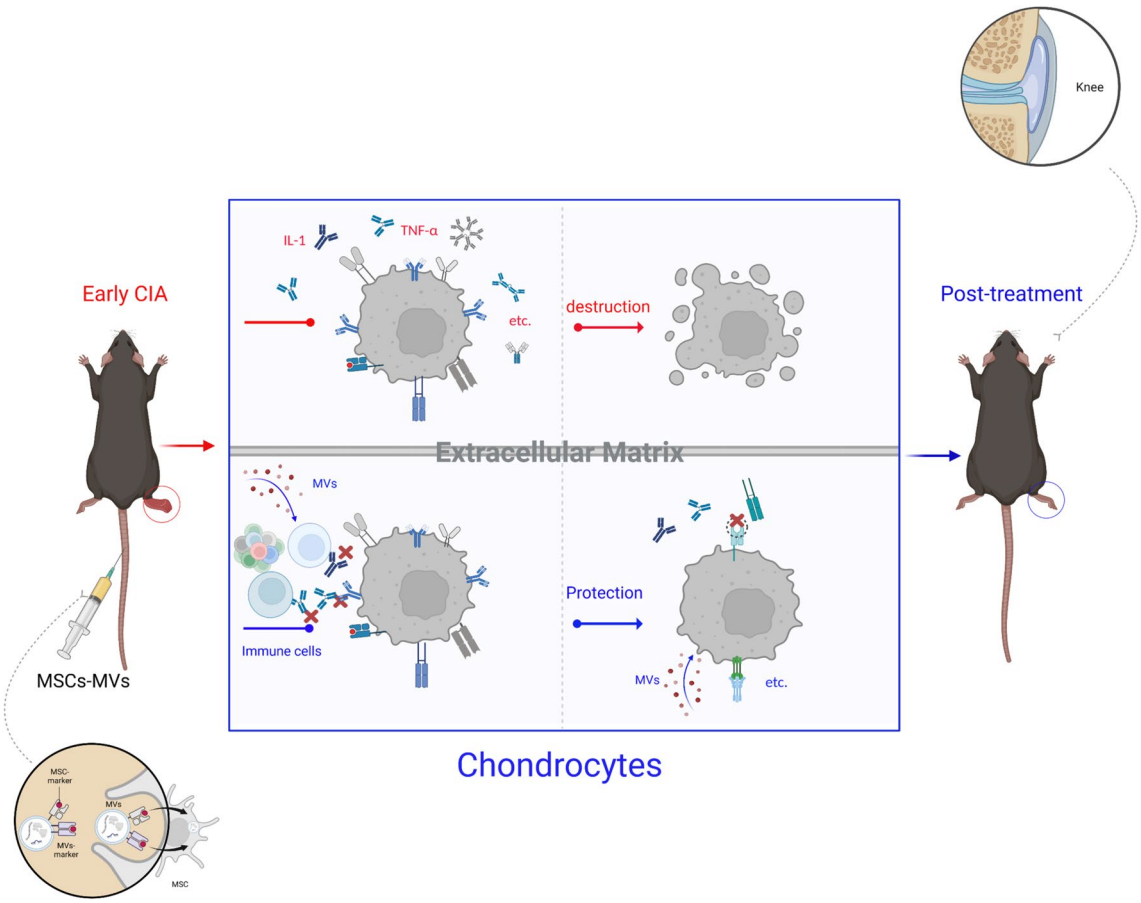

Background

Rheumatoid arthritis (RA) is an erosive, symmetrical, immune-mediated polyarthritis of unknown etiology [1, 2]. The primary pathogenic process involves the disruption of immune tolerance, leading to the activation of immune cells and the production of autoantibodies, which subsequently result in damage to the joints and other body systems. RA affects approximately 18 million people worldwide [3]. In 2012, the concepts of early RA and preclinical RA (pre-RA) were introduced by the American College of Rheumatology (ACR) [4–6]. Research on early and pre-RA showed that earlier treatment significantly improves patient outcomes. As a result, research on early or pre-RA is increasingly becoming a prominent area of interest in both clinical and basic research [7, 8].

Pre-RA can be divided into several stages. The at-risk stage is characterized by environmental factors (e.g., smoking and obesity) as well as genetic factors (e.g., MHC II and HLA-DR) contributing to the potential risk for RA development. Next, in the presymptomatic RA stage, autoimmunity is activated, leading to the production of autoantibodies [e.g., anti-cyclic citrullinated peptide antibody (ACPA), anti-collagen type II (anti-CII), and rheumatoid factor (RF)]. However, the patient remains asymptomatic, as arthritis has yet to develop. Finally, the activation of immune cells (T and B lymphocytes and neutrophils) results in proteoglycan depletion, cartilage destabilization, and the activation of synovial cells [9, 10]. This stage is also known as the critical "window period" for RA treatment.

Individuals who test positive for ACPAs are believed to have a 98% probability of developing RA within

2-10 years [11–14]. In individuals positive for ACPAs, magnetic resonance imaging (MRI) has shown that bone and cartilage inflammation occurs earlier than synovitis [15, 16]. Histological analysis of synovial tissue from ACPA-positive individuals in the pre-RA stage also revealed no notable abnormalities [17]. Clinically, bone and joint pain tend to manifest earlier in ACPA-positive individuals. Furthermore, MRI scans of ACPA-positive individuals experiencing joint pain but without arthritis distinctly indicated localized subclinical inflammation [18]. In these patients, while synovial hyperplasia was absent, inflammation in the cartilage and bone was still detectable [19, 20]. Therefore, in the management of pre-RA, maintaining cartilage homeostasis is crucial and takes precedence over the concerns typically associated with late-stage chronic arthritis.

Mesenchymal stem cells (MSCs) have gained widespread attention in the field of cell therapy [21] and have been used to treat rheumatic diseases, including RA [22]. Recent research has particularly explored the paracrine effects of MSCs [23–25], highlighting the roles of extracellular vesicles, such as exosomes (exos) and microvesicles (MVs), which can partially or completely mimic the functions of their originating cells [26]. MVs have effects similar to those of MSCs in terms of immunomodulation, alleviation of degenerative conditions, and maintenance of cartilage homeostasis [27]. However, the mechanism by which MSC-MVs protect cartilage in early RA is poorly understood. In this study, we investigated the therapeutic effect of MVs on early collagen-induced arthritis (CIA).

Methods

Reagents and cells

Human chondrocyte CP-H096 (Pricella, China), C28/I2 (Sigma, USA), and mouse chondrocyte CP-M087 cells (Pricella, China) were cultured in Dulbecco's modified Eagle's medium (DMEM, Gibco, 11960044) supplemented with 100 μg/mL penicillin/streptomycin (Gibco, 15140122), 2 mmol/mL glutamine (Gibco, 25030081), and 10% fetal bovine serum (FBS, Gibco, 10099-141C). Mouse peripheral blood mononuclear cells (PBMCs) were isolated from DBA/1J mouse whole blood and cultured in DMEM supplemented with 100 μg/mL penicillin/streptomycin, 2 mmol/mL glutamine, and 10% FBS. Chondrocytes from 3 RA patients were donated and collected from the patients during surgery. Ethical approval for this study was obtained from the Biomedical Ethics Committee of West China Hospital, Sichuan University (Approval Number: 1771, Date: December 22, 2022). All procedures performed in studies involving human participants were in accordance with the ethical standards of the institutional and/or national research committee and with the 1964 Helsinki Declaration and its later amendments or comparable ethical standards.

MSC culture and identification

MSCs originating from 2 healthy human donors (No. 2020509, 2020510) were sourced from the Chengdu Stem Cell Biobank. Prior to and upon storage, the MSCs underwent comprehensive analyses, including endotoxin testing (detection number: JK-ZK-SR-005). The MSCs were cultivated in proliferative medium composed of α-MEM (Gibco, C12571500BT), 100 μg/mL penicillin/streptomycin, and 2 mol/mL glutamine and supplemented with 10% FBS. The cells were passaged upon reaching 80–90% confluence. The MSCs used in the experiments were from passages 5 to 7. All the cells were incubated at 37 °C with 5% CO_2. Surface marker analysis of MSCs (PE CD44, FITC CD90, PerCP-Cy™5.5 CD105, and APC CD73) was performed via flow cytometry following the manufacturer's instructions (BD Stemflow™, AB_2869404). The potential of MSCs to differentiate into osteoblasts, chondrocytes, and adipocytes was evaluated via trilineage differentiation assay kits (MesenCult™-ACF Plus Medium, Stem Cell) according to the manufacturer's instructions.

MSC–MV extraction and identification

MVs were isolated via gradient centrifugation. MSCs were cultured for 48 h, followed by incubation in FBS-free medium for an additional 48 h to obtain supernatants. The collected supernatants were centrifuged at 300×*g* for 10 min and 2500×*g* for 20 min to eliminate cellular debris and apoptotic vesicles and subsequently at 50,000×*g* for 2 h to eliminate exos (Avanti JXN-26). The pellet was resuspended in PBS (Gibco™, C10010500BT) and centrifuged at 50,000×*g* for 2 h. This process was repeated three times. The size and morphology of the MVs were assessed via transmission electron microscopy (TEM), whereas the particle size and number were determined via ZetaView (Particle Metrix, DEU). The expression of the MV membrane markers PE-CD44, APC-CD73, FITC-CD90, and PerCP-Cy™5.5-CD105 was analyzed via flow cytometry, and the expression of the vesicle markers CD63 and Annexin V was examined via Western blotting.

CIA induction and treatment

Male DBA/1J mice (n = 42), aged 6-7 weeks, were procured from Beijing Huafu Kang Biological Technology Co., Ltd. (Beijing, China), and acclimated for 1 week. All the mice were housed in ventilated cages with sterile food and ample water throughout the study, ensuring humane care in accordance with the institutional guidelines of Sichuan University. The animal protocol (Approval

Number: 2020285A; date of approval: 20200922) was reviewed and approved by the Animal Ethics Committee of Sichuan University. Purified collagen (Chondrex, #20022) was dissolved in 0.05 M acetic acid to achieve a final concentration of 2 mg/mL, followed by gentle stirring and overnight storage at 4 °C. Ultrasonication was conducted on ice (power 30%, working 3 s, pause 3 s, total time 5 min) after the addition of adjuvants until the emulsifier droplets stopped dispersing in the water. Subsequently, 0.1 mL of the emulsifier [50 μL of CFA (Chondrex, #7009)/IFA (Chondrex, #7002) + 50 μL of CII CAS] was injected into the tail base of each mouse on days 0 and 21. On day 22, the treatment group (n = 6) received intravenous injections of MVs at a dosage of 10^8/100 μL once a week for 4 weeks. In the CIA group (n = 6 × 4), four animals were euthanized at 21 (21-CIA group), 23 (23-CIA group), 25 (25-CIA group), and 45 days. PBS (100 μL of PBS) was administered intravenously once a week for 4 weeks. Starting at 21 days, the mice were scored once every 2 days according to Table 1. The control group (n = 6 × 2; 2 control animals were euthanized at 21 and 45 days) did not receive any intervention.

In vivo bioluminescence imaging

MVs (10^8 per 100 μL) labeled with DiI dye (Invitrogen, # D3911) were injected into the mouse tail vein to observe the metabolism of the drug. After 24 h, the mice were anesthetized and positioned on animal plates. Imaging was performed using an IVIS Spectrum in vivo imaging system (PerkinElmer; Living Image software), and the excitation wavelength was set to 740 nm. After imaging, the mice were euthanized, and the tissues were cryopreserved in liquid nitrogen. Frozen tissue sections were sliced and examined under a fluorescence microscope to evaluate the distribution of MVs.

Microcomputed tomography (micro-CT)

After 45 consecutive days of MV treatment, all the mice were anesthetized with isoflurane, and their hind limbs were freshly harvested and fixed in 4% paraformaldehyde. Micro-CT was performed via a Quantum GX micro-CT Imaging System (PerkinElmer, USA) to assess the extent of bone destruction and osteoporosis. The scanning parameters were as follows: X-ray voltage, 90 kV; X-ray current, 88 μA; field of view (FOV), 25 mm; and stereoscopic pixels (pixel size), 50 μm. Images were analyzed via 12.0 micro-CT analysis software (PerkinElmer, USA) for 3D reconstruction of the foot claw and knee joint, and a 2 mm section distal to the tibial diaphysis (40-layer image) was selected as the target range. The volume was measured, and trabecular number (Tb) and count of trabeculae (N) were calculated and quantified for comparative analysis.

Histological staining

After fixation with 4% paraformaldehyde for 24 h, the samples were embedded, sectioned, and stained with hematoxylin and eosin (H&E), safranin O-fast green, Masson's trichrome, and tartrate-resistant acid phosphatase (TRAP). Subsequently, slide analysis was conducted via a 3D Histech microscope (QuantCenter image analysis solutions), Halo AI (Indica Labs), and QuPath software (Quantitative Pathology).

Enzyme-linked immunosorbent assay (ELISA)

After euthanasia, blood was collected from the mouse orbital vein and centrifuged at 1000×*g* at 4 °C for 10 min to obtain the serum. The serum concentrations of TNFα, IL-1β, IL-17A, IL-10, and IL-6 were determined via ELISA kits following the manufacturer's instructions. All the ELISA kits used were from Abcam (Cambridge, MA, USA), and the experiments were conducted in triplicate. The cell supernatant was assayed via the same method used for serology.

Flow cytometric analysis

Lymph and spleen tissues were minced, digested via Liberase (Roche), and filtered through a 70 μm mesh to obtain single-cell suspensions. Fixation with Intracellular (IC) Fixation Buffer (eBioscience) was performed according to the manufacturer's protocol. Flow cytometric analysis of Th1/2/17, Treg, Tfh, and B cells from the lymph and spleen involved both intracellular and extracellular staining. For Th1/2/17 staining, the cells were stimulated with 10% FBS RPMI-1640 + 30 μL PMA + 30 μL Ion + 30 μL Golgi inhibitor for 4-5 h. Surface staining

Table 1 Arthritis score for collagen-induced arthritis

Severity score	Degree of inflammation
0	No evidence of erythema and swelling
1	Erythema and mild swelling confined to the tarsal or ankle joints
2	Erythema and mild swelling extending from the ankle to the tarsal joints
3	Erythema and moderate swelling extending from the ankle to metatarsal joints
4	Erythema and severe swelling encompass the ankle, foot and digits, or ankylosis of the limb

with CD3e-APC-Cy7 (1.5 μL/tube) and CD4-PerCP-Cy5.5 (0.33 μL/tube) was performed, followed by fixation and permeabilization for intracellular staining with IFN-γ-FITC (0.5 μL/tube), IL-4-APC (0.625 μL/tube), and IL-17A-PE (0.625 μL/tube). For Treg staining, surface staining with CD3e-APC-Cy7 (1.5 μL/tube), CD4-PerCP-Cy5.5 (0.33 μL/tube), and CD25-BB515 (1 μL/tube) was followed by intracellular staining with FoxP3-APC (0.5 μL/tube) after membrane permeabilization. Tfh staining included CD45-AF700 (1:150), CD3e-APC-Cy7 (1.5 μL/tube), CD4-PerCP-Cy5.5 (0.33 μL/tube), CXCR5 (CD185)-APC (1:50), PD1 (CD279)-PE (1:50), and ICOS (CD278)-BV421 (1:50) staining. B cells were stained with CD19-BV510 (0.5 μL/tube) and IL-10-APC (1.25 μL/tube). All flow cytometric assays were conducted in a 50 μL system.

Quantitative real-time PCR (RT-qPCR)

Total RNA was extracted from cartilage tissues via TRIzol reagent (Invitrogen, Carlsbad, CA, USA) and converted into complementary DNA via iScript cDNA Synthesis kits (Bio-Rad, Shanghai, China) following the manufacturer's instructions. RT-qPCR was conducted via iQTM SYBR Green Supermix (Bio-Rad) in a 7500 HT Fast Real-Time PCR system (Applied Biosystems, Foster City, CA, USA). The primer sequences are provided in Table 2. Relative gene expression was determined via the $2^{-\Delta\Delta Ct}$ method, with β-Actin serving as the internal reference. The experiments were performed in triplicate. For determination of the Ct values, these values were normalized to the endogenous reference (ΔCt = Ct target − Ct β-actin) and compared with a calibrator and the ΔΔCt method (ΔΔCt = ΔCt test sample − ΔCt calibrator sample).

Western blotting analysis

Radioimmunoprecipitation assay (RIPA) lysis buffer (Beyotime, China) was used for the lysis of cells or cartilage tissue over a 15-min period. Bicinchoninic acid protein assays were employed to determine protein concentrations. Subsequently, equal amounts of protein were dissolved in Laemmli sample buffer, boiled for 5 min, subjected to SDS-PAGE and transferred onto polyvinylidene difluoride membranes. After being blocked with Tris-buffered saline-Tween containing 5% skim milk, the membranes were probed with primary antibodies [against MMP-13, ADAMTS-5, type I collagen (CI), and CII] overnight at 4 °C and subsequently incubated with the corresponding secondary antibodies for 1 h at room temperature. The protein bands were detected via enhanced chemiluminescence (ECL) (GE Healthcare, USA).

Table 2 Primer sequences for RT-qPCR

Primer name	F/R primer	Primer sequence
h-β-Actin	Forward primer	5′-ACTCTGTGTGGATTGGTGGC-3′
	Reverse primer	5′-GCTCAGTAACAGTCCGCCT-3′
h-IL-1β	Forward primer	5′-TGCCACCTTTTGACAGTGATG-3′
	Reverse primer	5′-TGATGTGCTGCTGCGAGATT-3′
h-TNFα	Forward primer	5′-GGTGCCTATGTCTCCAGCCTCTT-3′
	Reverse primer	5′-GCCATAGAACTGATGAGGGAG-3′
h-MMP-13	Forward primer	5′-TTTGAGAACACGGGGAAGA-3′
	Reverse primer	5′-ACTTTGTTGCCAATTCCAGG-3′
h-ADAMTS-5	Forward primer	5′-CTDCCTTCAAGGCAAATGTGTGG-3′
	Reverse primer	5′-CAATGGCGGTAGGCAAACTGCA-3′
m-β-Actin	Forward primer	5′-AGATGTGGATCAGCAAGCAG-3′
	Reverse primer	5′-CGCTCAGGAGGAGCAATG-3′
m-IL-1β	Forward primer	5′-GAAATGCCACCTTTTGACAGTG-3′
	Reverse primer	5′-TGGATGCTCTCATCAGGACAG-3′
m-TNFα	Forward primer	5′-GAGGCCAAGCCCTGGTATG-3′
	Reverse primer	5′-CGGGCCGATTGATCTCAGC-3′
m-MMP-13	Forward primer	5′-AGAATCTATGATGGCACTG-3′
	Reverse primer	5′-TGTAGCCTTTGGAACTG-3′
m-ADAMTS-5	Forward primer	5′-GCCAGGC GGATGTGGTTCTCAA-3′
	Reverse primer	5′-ATGCGGCTCGAGTGGGCGCCCT TGT-3′
m-Collagen I	Forward primer	5′-AAGAACCCTGCCCGCACATG-3′
	Reverse primer	5′-GAATCCATCGGTCATGCTCT-3′
m-Collagen II	Forward primer	5′-ATGCTGCTGCTGCTGCTG-3′
	Reverse primer	5′-AGGCTGCTGCTGCTGCTG-3′

m mice, *h* human

Transwell assays

The upper layer was overlaid with PBMCs, which were then stimulated with 1 μg/mL of lipopolysaccharide (LPS) for 1 h before being transferred onto a 24-well plate preseeded with 10^6 chondrocytes. Coculture was maintained for 24 h, after which the medium, PBMCs and chondrocytes were collected for further analysis.

Immunofluorescence and immunohistochemistry

After deparaffinization in water, the tissue sections were incubated overnight at 4 °C with primary antibodies. For nonconjugated primary antibodies, the sections were subsequently incubated at room temperature with Alexa Fluor 488/546-conjugated secondary antibodies (1:1000, Invitrogen) in staining buffer (Invitrogen) for 2 h. Nuclear staining was achieved via the use of Hoechst 33342 or DAPI, followed by sealing with PermaFluor mounting medium (Thermo Fisher Scientific). Confocal laser scanning microscopy was used to capture images. Immunofluorescence staining of the cells was performed using phalloidin, PKH26, and Hoechst 33342 or DAPI

(Thermo Fisher Scientific, USA). For immunohistochemistry, tissue sections were immersed in sodium citrate buffer (10 mM, pH 6.0) and subjected to heat retrieval for 20 min in a 100 °C water bath to facilitate antigen retrieval. The slices were then permeabilized and blocked in PBS-T (0.03% Triton X-100) containing 1% goat serum for 1 h at room temperature. The tissue sections were incubated overnight at 4 °C with antibodies against IL-1β, TNFα, IL-6, IL-17, ADAMTS-5, MMP-13, CI, CII, and aggrecan (ABclonal, China), followed by incubation with horseradish peroxidase-conjugated goat anti-rabbit IgG. Normal rabbit IgG (ABclonal, China) was used as a histological control. Immunohistochemical staining was visualized via DAB (Zhongshan Biotech, Beijing, China, #ZLI-9032). Images were analyzed via Halo AI and QuPath.

Proliferation, migration and apoptosis assays

For cell proliferation assays (CCK-8 assays), the cells were seeded in a 96-well plate. The cells were treated as indicated. CCK-8 reagent was added, and the samples were incubated. The absorbance was measured at 450 nm. For cell migration assays (scratch assay), a scratch was created in a confluent monolayer. The cells were treated as indicated. The scratch closure was observed over time. Then, the migratory distance was determined. For cell apoptosis analysis (flow cytometry), cells were treated with the test compounds. Then, the samples were stained with Annexin V and PI and analyzed by flow cytometry. The number of apoptotic and necrotic cells was quantified on the basis of the staining patterns.

Whole-transcriptome sequencing

For RNA extraction, TRIzol was used to lyse the cells. The mixture was allowed to stand for 15 min to lyse the cells, 200 μL of chloroform was added, the mixture was vortexed for 15 s, and the mixture was allowed to stand for 3 min. The mixture was subsequently centrifuged at 4 °C at 13,000 r/min for 15 min, the supernatant was aspirated into a new EP tube without RNA, an equal volume of isopropanol was added, the mixture was gently inverted and mixed, and the mixture was allowed to stand for 10 min at room temperature. After 10 min, the mixture was centrifuged at 4 °C for 15 min at 13,000 r/min, and the supernatant was discarded. After another 10 min, the mixture was again centrifuged at 4 °C for 15 min at 13,000 r/min, the supernatant was discarded and the mixture was placed on the ventilating table to dry until the RNA became transparent. A total of 20 μL of DEPC water was added to dissolve the RNA sample. For data analysis, after the raw data for sequencing (raw data) were obtained, the raw data were first filtered to obtain high-quality sequencing data (clean data), and the sequencing data (clean data) were compared with the reference genome of the project species to obtain comprehensive transcript information and perform gene expression quantification, as well as Gene Ontology (GO) and Kyoto Encyclopedia of Genes and Genomes (KEGG) pathway analysis.

Statistical analysis

In this study, the data are expressed as the means ± SDs or percentages. Statistical values for the in vitro experiments were derived from at least 3 independent experiments. Comparisons between two groups were conducted via a 2-tailed Student's t test, whereas comparisons involving three or more groups were performed via one-way ANOVA followed by Bonferroni post hoc comparisons. P values < 0.05 were considered statistically significant. All the statistical analyses were conducted via GraphPad Prism 9 software (San Diego, California, USA).

Isolation, validation and safety assessment of MSCs and MSCs-MVs

Fourth-generation MSCs were obtained from a biological cell bank (Fig. 1a). Upon passaging, the cells were assessed for their stem cell characteristics, including morphology (Fig. 1b); the surface markers CD44, CD73, CD90, and CD105 (Fig. 1c); and trilineage differentiation potential (Fig. 1d). The cells from the fifth generation were cultured initially in FBS-containing medium for 48 h, followed by a subsequent 48-h culture in FBS-free medium. Using the method illustrated in Fig. 1e, we isolated MVs from the culture medium. Nanotracking and TEM analyses confirmed that the size range of the majority of the particles was 100–1000 nm, indicating a vesicular structure (Fig. 1f, g). Membrane marker profiling revealed the expression of the MSC markers CD44, CD73, CD90, and CD105 on MVs (Fig. 1i). Additionally, Western blotting revealed the presence of the extracellular vesicle markers CD63 and Annexin V in the MVs (Fig. 1h). These results indicate that the method outlined in the schematic diagram successfully isolated the MVs required for subsequent experiments. In vivo studies involved the intravenous injection of 10^8/100 μL of MVs into DBA/1J mice twice a week for 3 consecutive months to assess the safety of MVs as therapeutic agents (Fig. S1a). Throughout the 3-month in vivo study period, no mortality was observed in the mice injected with MVs (Fig. S1b), and no apparent adverse effects were noted. Dissection of major organs revealed no pathological abnormalities (Fig. S1c). Metabolic tracing revealed that MVs can be transported intravenously to cartilage, major organs (with clustering observed in the red pulp of the spleen), and throughout the body within 1 h and are metabolized

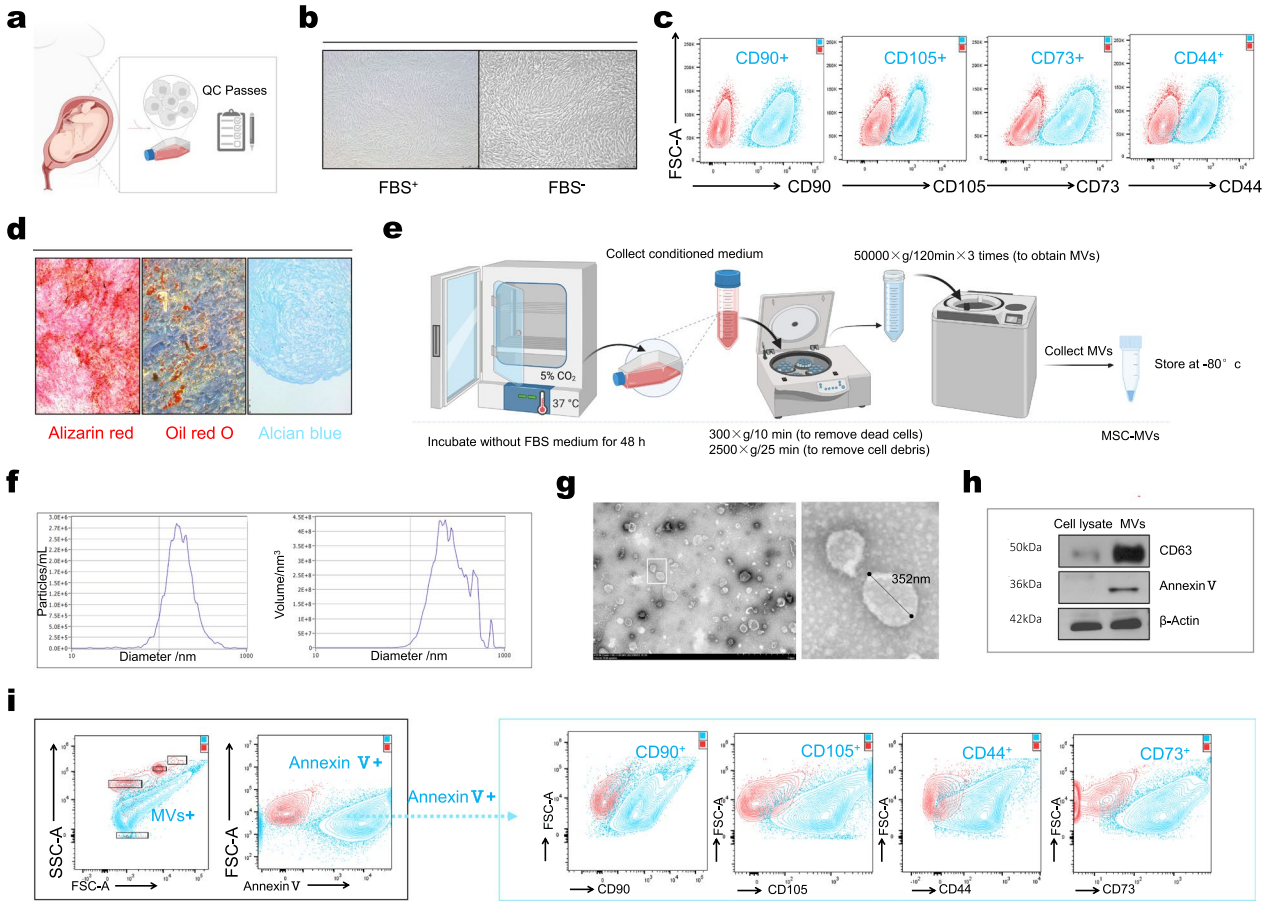

Fig. 1 Acquisition and identification of MSCs and MVs. **a** Acquisition and quality control (QC) of MSCs were performed with the Chengdu Stem Cell Biobank. **b** Morphology of MSCs in media supplemented with FBS and serum starved for 48 h. **c** MSC membrane markers (CD44, CD73, CD90, and CD105) were identified via flow cytometry. **d** The osteogenic (Alizarin red), adipogenic (Oil red O), and chondrogenic (Alcian blue) differentiation potential of MSCs. **e** An experimental protocol for the isolation of MVs via differential ultracentrifugation was implemented. **f** The size and number of MVs were measured via ZetaView. **f** Size and shape were analyzed via TEM. **h** Protein identification of MVs (CD63 and Annexin V) was performed via Western blotting. **i** Membrane markers of MVs (CD44, CD73, CD90, and CD105) were identified via flow cytometry

within 7 days. Toxicity assessments revealed that MVs could enter chondrocytes (Fig. S1d, e) without inducing cellular abnormalities; CCK-8 assays revealed no cellular toxicity (Fig. S1f, g). These findings collectively support the safety profile of MVs as therapeutic agents.

Collagen loss occurs early in mice with CIA

On day 0 and day 21, the mice received 2 doses of CFA with CII CAS (Fig. 2a). By day 25, a subset of the mice had developed arthritis, with a significant increase in the number of inflamed joints and CIA scores compared with those of the control group ($P < 0.001$) (Fig. 2b–d). CT

(See figure on next page.)

Fig. 2 Lesions of joints from mice with early CIA. **a** Experimental design. **b** Following the conclusion of the 21-day modeling period, arthritis onset in mice was observed between days 21 and 25. **c** Arthritis scores recorded from 21 to 25 days. **d** Frequency of arthritis episodes occurring between 21 and 25 days. **e** Changes in cartilage thickness observed via CT imaging from 21 to 25 days. **f** Histological assessment of knee joint sections stained with H&E on days 21, 23, and 25 to evaluate the cartilage area and damage scores. The scoring criteria were as follows: 0—no damage, 1—mild cartilage damage, and 2—severe cartilage damage or absence of articular cartilage due to arthritis. **g** Sections from mice with CIA stained with safranin O/fast green were used to evaluate cartilage destruction, bone erosion and collagen loss. **h** Masson-stained sections from mice with CIA were used to evaluate collagen loss. **i** Analysis of alterations in CII in joints from 21 to 25 days via immunohistochemistry. The positive areas of the sections were calculated with Halo AI. The data are presented as the means ± SDs. All the data were analyzed via one-way ANOVA followed by Tukey's post hoc test. Two-tailed P values < 0.05 were considered significant. $P < 0.05$, $P < 0.01$, $P < 0.001$, $P < 0.0001$

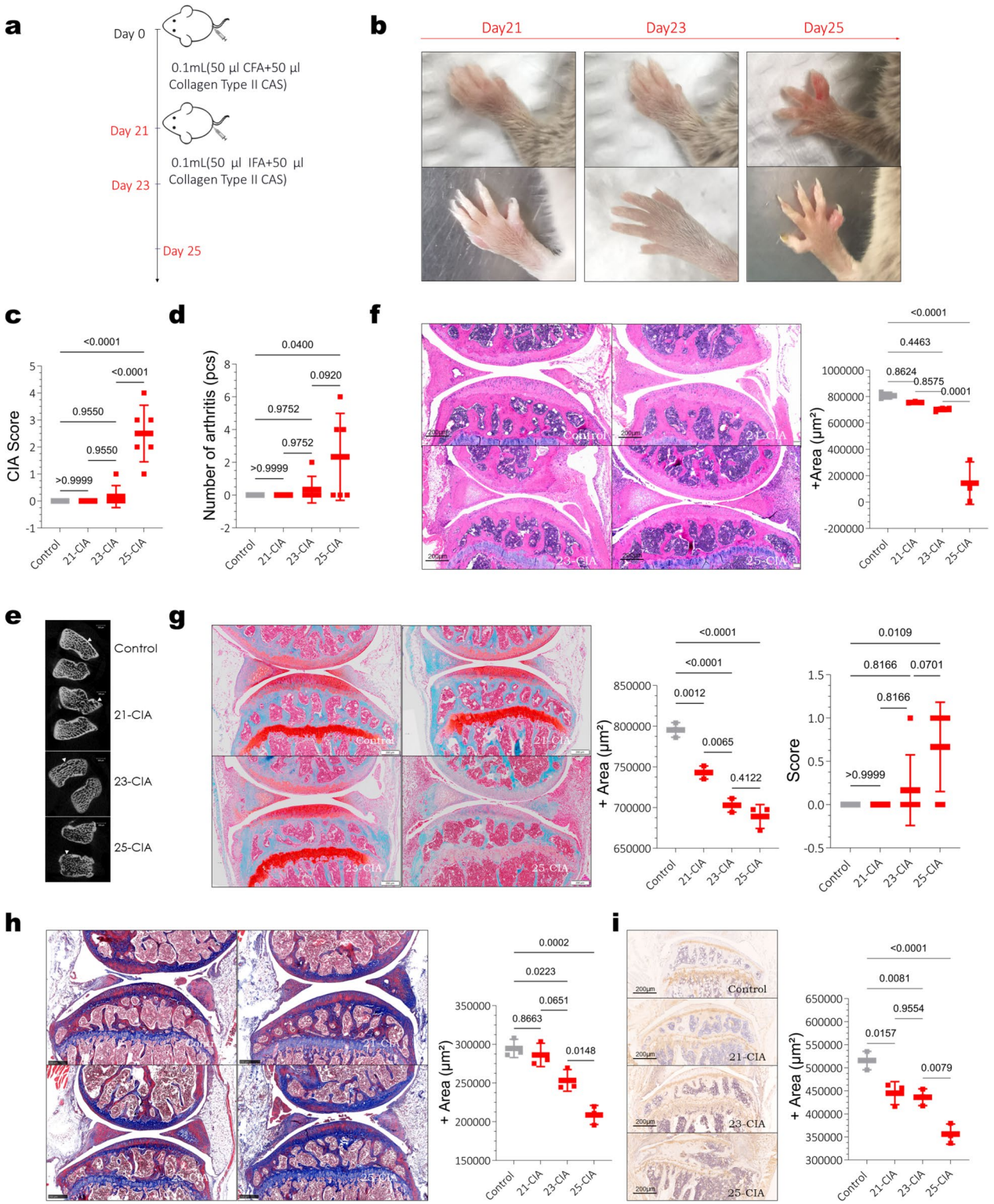

Fig. 2 (See legend on previous page.)

images revealed thinning of the articular cartilage and a decrease in trabecular bone (Fig. 2e). Histopathological analysis of H&E-stained sections revealed that at 21 and 23 days, compared with those in the control group, the mice in the experimental group presented receding cartilage tide lines and no notable synovial hyperplasia. However, by day 25, the mice showed no major joint destruction but an increased presence of synovial membranes. Concurrently, there was a decrease in the cartilage area ($P < 0.01$) and an increase in the joint destruction score ($P < 0.05$) (Fig. 2f). An evaluation of red-solid green staining revealed that the cartilage tide line receded, red collagen levels decreased, and notable changes occurred in the cartilage of the mice at 21 and 23 days. In contrast, at 25 days, the mice displayed evident cartilage erosion (Fig. 2g). Masson staining further confirmed a gradual reduction in red collagen levels compared with those in the control group, with a prominent decrease observed on day 25 (Fig. 2h). Immunohistochemistry revealed a gradual decrease in CII levels (Fig. 2i). TRAP staining revealed increased osteoclasts in the subchondral bone (Fig. S1h). These findings from the early stages of CIA suggest that collagen loss in the articular cartilage occurs before notable synovial proliferation.

MVs reduce inflammation in mice with early CIA

MVs were intravenously administered to the mice with CIA once a week for four treatments starting on day 22 (Fig. 3a). CIA scoring commenced on day 21 to evaluate arthritis progression. In the treatment group, the degree of arthritis remained stable, whereas the CIA group presented elevated CIA scores (Fig. 3b). The weights of the mice with CIA continued to decrease after 21 days, whereas the weights of the mice treated with MVs initially decreased but then recovered (Fig. 3c). H&E staining of major organs from all the treated mice revealed no effect of MVs on vital organ morphology (Fig. S1i), indicating the safety of the treatment. In vivo fluorescence imaging revealed enriched MVs near inflamed joints following intravenous administration of MVs (Fig. 3d). Statistical analysis revealed a significant correlation between inflammation and enriched fluorescence ($P = 0.0003$ and $P = 0.0257$) (Fig. 3e), suggesting that MVs accumulate at highly inflamed joints to exert their effects. Flow cytometric analysis of the lymph nodes and spleen revealed increased Tfh and Th1/17 cell populations in the mice with CIA, which were reduced in the MV group. In contrast, the Treg and Th2 cell populations decreased in the CIA group but increased in the MV group. In B cells, the number of $CD19^+$ and $IL\text{-}10^+$ cells decreased in the mice with CIA but increased after MV treatment, which was consistent with the findings in the lymph node and spleen (Fig. 3f). Spleen staining with CD4 and CD19 antibodies revealed significantly increased expression of CD4 and CD19 in the mice with CIA, which is indicative of T and B-cell activation. After MV treatment, CD4 and CD19 expression in the spleen decreased (Fig. 3g). Spleens from the mice with CIA also presented high expression of IFNγ and IL-17, which were expressed at low levels in the MV-treated mice. The number of T cells expressing IL-4 increased after MV treatment (Fig. 3h). Consistent with the flow cytometric results, analysis of serum inflammatory factors via ELISAs revealed elevated levels of IL-1β, TNFα, IL-6, and IL-17A in the CIA group. These levels were lower in the MV-treated group than in the CIA group but remained higher than those in the control group (Fig. 3i). RNA extraction and quantitative analysis via real-time polymerase chain reaction (RT-qPCR) of mouse articular cartilage revealed increased expression of IL-1β and TNFα in the mice with CIA, which was lower than that in the MV-treated group. However, no significant differences in IL-6 expression were observed among the three groups (Fig. 3j). Histochemical staining revealed increased IL-1β and TNFα levels in the cartilage region of the CIA group, whereas these levels were lower in the MV group than in the CIA group (Fig. 3k, l). Notably, IL-6 and IL-17 were not detected in the cartilage (Fig. S1l). These results indicate that MVs can reduce systemic inflammation in mice with CIA.

MVs reduces cartilage destruction in early CIA model mice

Micro-CT analysis revealed lower bone density and fewer trabeculae in the CIA group than in the control group ($P = 0.0007$). However, in the CIA group treated

(See figure on next page.)

Fig. 3 MVs alleviate inflammation in joints and systemically. **a** Experimental design. **b** CIA scores recorded from days 21 to 45. **c** Mouse body weights were recorded from days 21 to 45. **d** Bioluminescence imaging of mice injected with MVs and Dil dye. **e** Quantification of fluorescence intensity (ctrl vs. CIA, $P = 0.0003$; CIA vs. CIA-MVs, $P = 0.0257$). **f** Flow cytometric analysis of T follicular helper (Tfh^+), regulatory T ($Treg^+$), T helper ($Th1/2/17^+$), and B ($CD19^+$ and $IL\text{-}10^+$) cells in the lymph and spleen. **g** Alterations in splenic T ($CD4^+$ red) and B ($CD19^+$ green) cell populations. **h** Immunofluorescent spleen [IFNγ (red-Th1), IL-4 (green-Th2) and IL-17 (pink-Th17)] analysis was used to observe the distribution and number of Th1/2/17 cells. **i** Measurement of IL-1β, IL-6, TNFα, IL-10, and IL-17A expression in mouse serum via ELISAs. **j** RT-qPCR analysis of IL-1β, IL-6, and TNFα expression in articular cartilage. **k** IL-1β expression in articular cartilage. Analysis with Halo AI. **l** TNFα expression in articular cartilage. Analysis with Halo AI. Statistical analysis was performed via one-way ANOVA followed by Tukey's post hoc test. Two-tailed P values < 0.05 were considered significant. $P < 0.05$, $P < 0.01$, $P < 0.001$, $P < 0.0001$

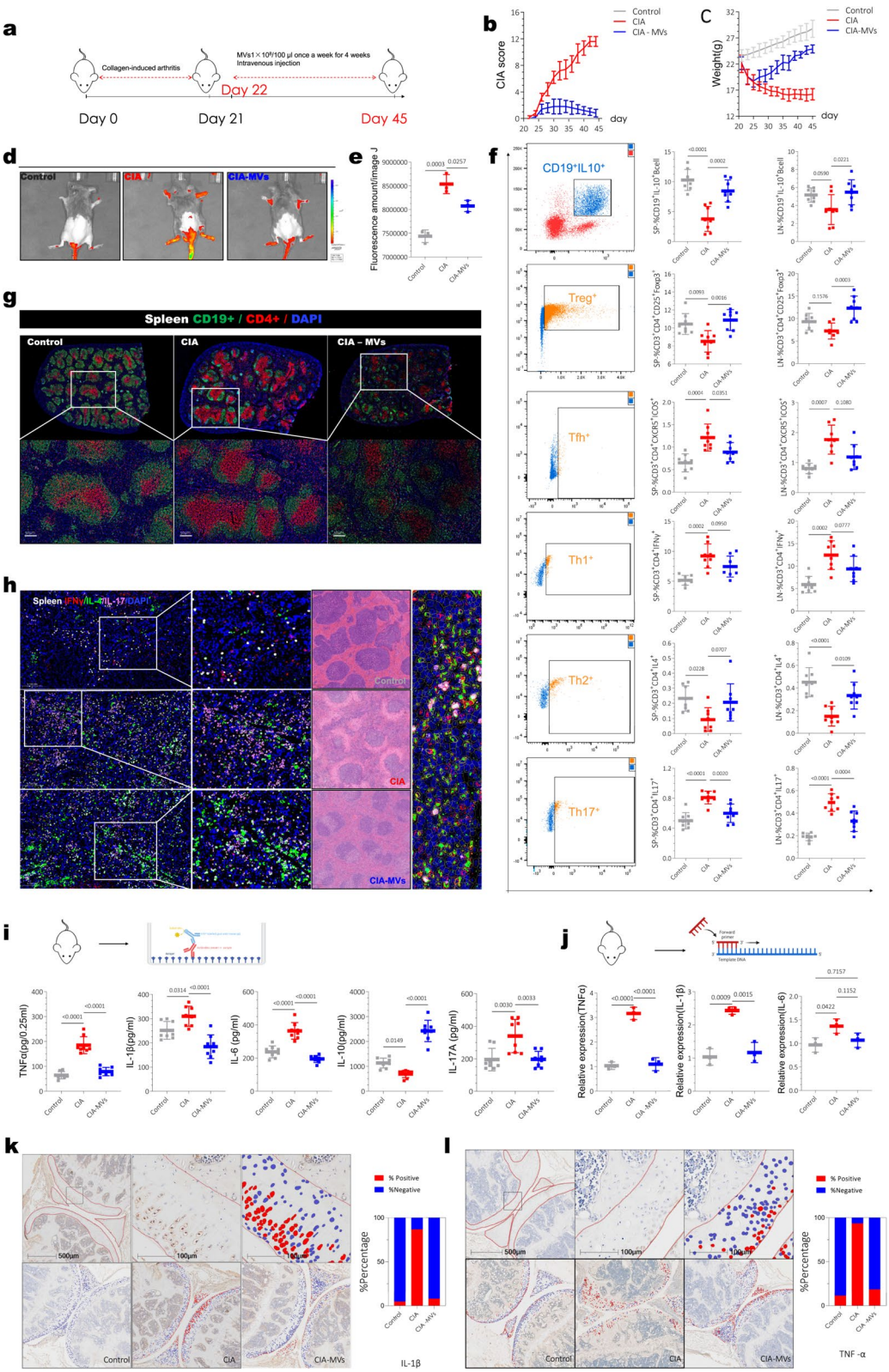

Fig. 3 (See legend on previous page.)

with MVs, there was a trend toward recovery in terms of bone density and the number of trabeculae; however, this difference was not statistically significant (P = 0.1107). Compared with those of the control group, 3D CT reconstruction revealed evident cartilage and bone destruction in the knee and ankle joints of the CIA group. Conversely, the MV treatment group presented smoother joint surfaces without notable damage. Statistically significant differences in 3D joint surface scores and Tb were observed (P < 0.05) (Fig. 4a). After the articular cartilage was ground, protein extraction and western blotting were performed. The CIA group presented high expression of ADAMTS-5 and MMP-13, along with decreased expression of CI and CII. In the treatment group, we found reduced expression of ADAMTS-5 and MMP-13, thereby protecting collagen from degradation (Fig. 4b). These findings were further validated by RT-qPCR, which yielded results consistent with those of the western blot analysis (Fig. 4c). H&E staining revealed notable synovial hyperplasia, decreased cartilage thickness, and anterior displacement of the tidemark in the CIA group (Fig. S1j). In contrast, compared with the control group, the treatment group exhibited only slight synovial hyperplasia and minimal changes in cartilage (Fig. S1k). Immunohistochemical staining of joint sections revealed an increased number of ADAMTS-5- and MMP-13-positive chondrocytes in the CIA group. The treatment group and control group presented fewer ADAMTS-5- and MMP-13-positive chondrocytes, although they were still present (Fig. 4e, f). Immunohistochemical staining of joint sections for CI and CII in the control group revealed that CII was located mainly in the middle of the cartilage, whereas CI was observed at the base. In the CIA group, CI migrated to the joint surface, indicating cartilage dissolution and exposure of CI, accompanied by a reduction in the amount of CII. Compared with the control group, the treatment group showed no significant difference, with slight changes in the localization of CI and CII in some areas of the cartilage (Fig. 4g, h). Aggrecan staining of joint sections revealed a significant reduction in aggrecan in the CIA group, whereas the treatment group showed no significant difference compared with the control group (Fig. 4i). MVs may act through the IL-1β/TNFα/MMP-13/ADAMTS-5 axis of cartilage destruction (Fig. 4j). These results indicate that MVs can reduce cartilage destruction in mice with CIA.

In vitro, MVs can reduce the activated inflammatory state

After the MVs (CFSE; green) were stained, they were washed and subjected to high-speed centrifugation. Then, the MVs were added to cultured chondrocytes for 24 h. After fixation with paraformaldehyde, immunostaining was performed with the F-actin microfilament protein fluorescent dyes phalloidin (red) and Hoechst (blue), which revealed MVs within the cells (Fig. 5a). For the Transwell experiments, chondrocytes and MVs were added to the bottom chamber, while PBMCs and LPS were added to the upper chamber. Immunofluorescence staining for IL-1β and TNFα revealed increased expression in the LPS group, whereas the LPS+MVs group presented no significant differences in expression. The cell supernatants were subjected to ELISA analysis after sonication, and the results were consistent with those of the immunofluorescence staining (Fig. 5b). LPS stimulation increased the expression of IL-1β, TNFα, IL-6, and IL-17A, whereas LPS stimulation in the presence of MVs resulted in decreased expression of these cytokines (Fig. 5c). Lysis and PCR analysis of the bottom chondrocytes revealed that MVs can reduce the levels of IL-1β and TNFα on the cartilage surface. In chondrocytes, stimulation with IL-1β or TNFα separately led to increased expression of the corresponding cytokines. After cell sonication, ELISAs of the cell suspensions confirmed the increase in TNFα expression in the IL-1β group and increased IL-1β expression in the TNFα group (Fig. 5d). The fluorescence immunostaining results were consistent with the ELISA results. RT-qPCR analysis of the cells yielded results consistent with the other findings (Fig. 5e, f). These results suggest that MVs can reduce immune inflammation and reduce IL-1β and TNFα in chondrocytes.

In vitro, MVs protect chondrocytes

Chondrocytes were obtained from RA patients who were treated with MVs, and cell migration was observed through scratch assays at 0 and 24 h. MVs clearly

(See figure on next page.)

Fig. 4 MVs maintain cartilage stability in mice with early CIA. **a** CT scans and 3D CT reconstruction of the mouse ankle and knee joints for the analysis of joint destruction and reduced trabecular bone. **b** Western blot analysis of ADAMTS-5, MMP-13, CI, and CII expression in mouse joint cartilage after cryogenic grinding. **c** RT-qPCR analysis of ADAMTS-5, MMP-13, CI, and CII expression in mouse joint cartilage. **d** Analysis of ankle and knee joint sections via safranin O–fast green staining. **e** Immunohistochemical staining of ADAMTS-5 in mouse knee joints. Analysis with Halo AI. **f** Immunohistochemical staining of MMP-13 in mouse knee joints. Analysis with Halo AI. **g** Staining of CII in mouse knee joints. Analysis with Halo AI. **h** Staining of CI in mouse knee joints. Analysis with Halo AI. **i** Staining of aggrecan in mouse knee joints. Analysis with Halo AI. The data are presented as the means ± SDs or percentages and were analyzed via one-way ANOVA followed by Tukey's post hoc tests. Two-tailed P values < 0.05 were considered significant

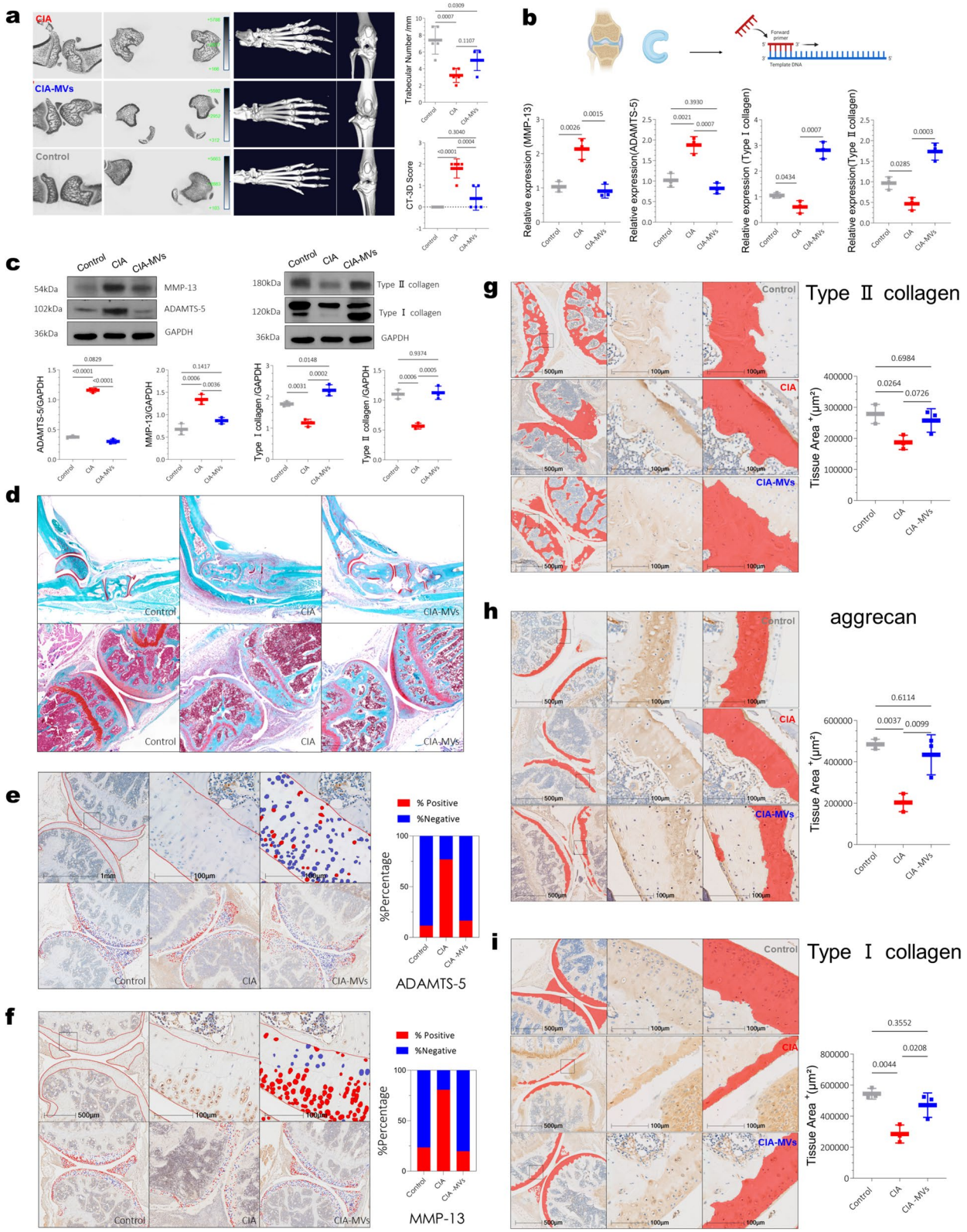

Fig. 4 (See legend on previous page.)

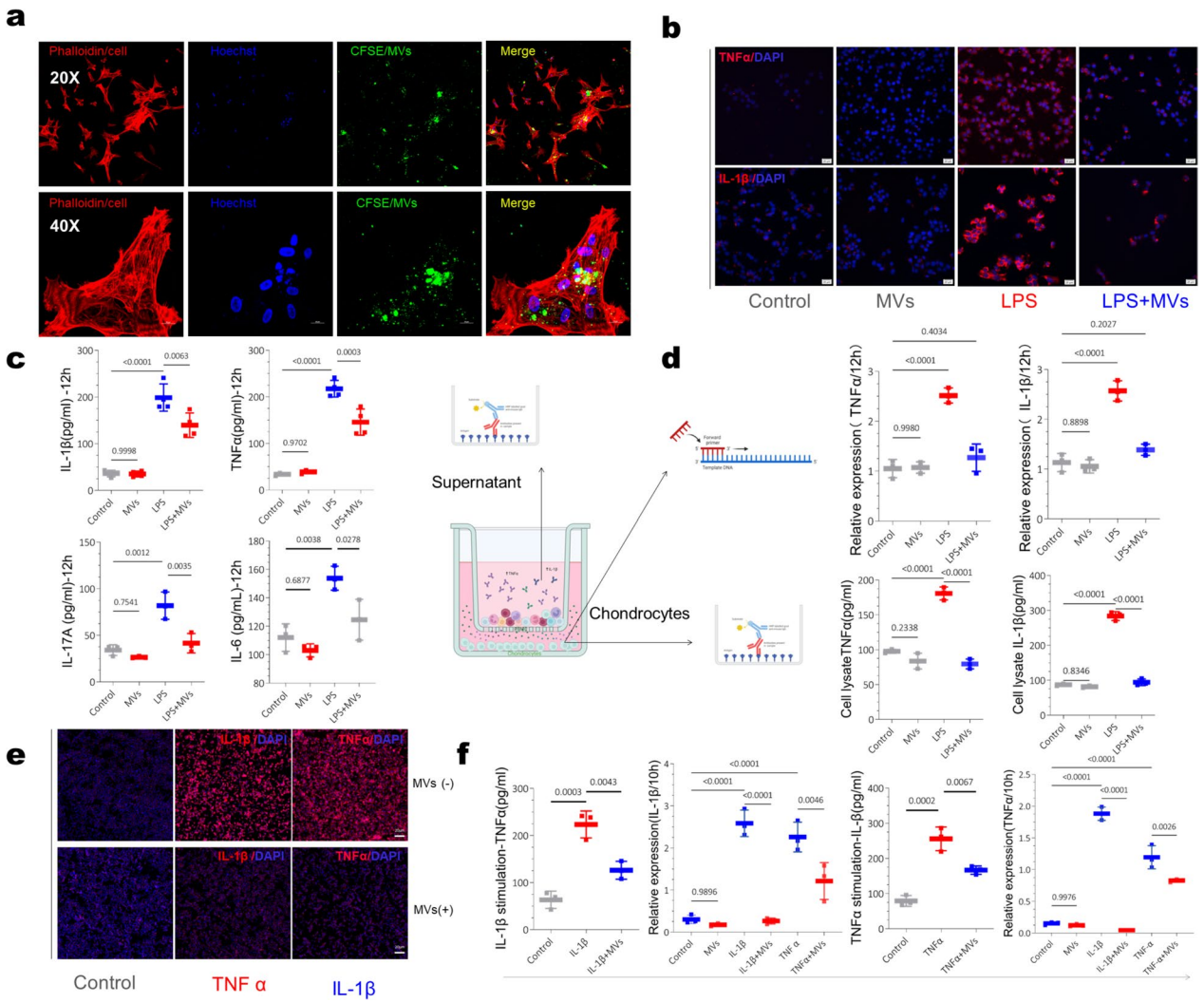

Fig. 5 Assessment of the anti-inflammatory effects of MVs in cells. **a** Observation of MVs entering chondrocytes via confocal microscopy (MVs-green-CFSE, cells-red-phalloidin, nuclei-blue-Hoechst). **b** Immunofluorescence analysis of IL-1β and TNFα expression in cartilage (IL-1β and TNFα-red, nucleus blue) from cocultured PBMCs and chondrocytes. **c** ELISA analysis of the expression of IL-1β, TNFα, IL-6, and IL-17A in the supernatant after MV intervention. **d** ELISAs and RT-qPCR analysis of the expression of IL-1β and TNFα in cartilage. **e** Immunofluorescence analysis of the expression of IL-1β and TNFα in chondrocytes after MV intervention (IL-1β and TNFα-red, nuclei-blue). **f** ELISAs and RT-qPCR analysis of IL-1β and TNFα expression in chondrocytes. The data are presented as the means ± SDs and were analyzed via one-way ANOVA followed by Tukey's post hoc tests. Two-tailed P values < 0.05 were considered significant

increased the migration of chondrocytes (Fig. 6a). After 12 h of passage, the addition of MVs resulted in a significant increase in cell proliferation at 48 h, as indicated by the red staining observed via the trypan blue method (Fig. 6b). The cells were cultured with MVs for 12 h, and subsequent flow cytometric analysis revealed a decrease in apoptosis in the dishes supplemented with MVs (Fig. 6c). Transcriptome sequencing was performed on both groups, and the analysis revealed the differential expression of 43 circRNAs, 101 miRNAs, and 45 lncRNAs. Thus, MVs may contribute to cellular repair and the alleviation of chondrocyte inflammation (Fig. 6d–f). As shown in Table 3, after treatment with IL-1β and TNFα, fluorescence immunostaining revealed reduced expression of ADAMTS-5 and MMP-13 in the MV group, which was consistent with the quantitative results obtained through RT-qPCR analysis (Fig. 6g, h). Similarly, immunofluorescence staining for CI and CII revealed that MVs maintained the expression of these collagen types. The Western blot results were consistent with the fluorescence immunostaining results (Fig. 6i–l).

Discussion

RA involves dysregulation of the immune system and pathological changes in cartilage at a very early stage. Controlling inflammation and cartilage destruction early on may be an effective approach for treating RA. MSCs are a class of cells characterized by self-renewal and multidirectional differentiation capabilities [28, 29]. Due to their unique functions, these cells have been extensively researched for the treatment of rare and challenging diseases [30]. Although several MSC-based products have received clinical approval, the complexity of cell therapeutic mechanisms and the uncertainties of potential risks have impeded the advancement and clinical application of stem cell therapy. Consequently, alternative research approaches have emerged, including preclinical studies involving MSC exos and MSC extracellular vesicles. These studies are based on the premise that nonimmunogenic exos and EVs carry therapeutic factors or proteins and have the potential to treat diseases [31–33]. Exos are vesicle-like structures released through exocytosis by fusing with the cell membrane and entering the extracellular space. Cellular MVs, which possess membrane structures, are similar to exos but are larger in diameter and richer in content [34]. In this study, we obtained MSCs from healthy human umbilical cords. These cells displayed typical MSC characteristics, such as the expression of the stem cell surface markers CD44, CD73, CD90, and CD105 and the potential for multilineage differentiation. MSC-MVs were obtained through stimulation and gradient centrifugation. We used electron microscopy to confirm their vesicular structure, and Western blot analysis confirmed the presence of the vesicular markers CD63 and Annexin. Flow cytometry also revealed that MVs retained their stem cell properties, as evidenced by their expression of surface markers characteristic of stem cells.

RA is a chronic autoimmune disease characterized by persistent joint inflammation and destruction. If left untreated, this condition leads to cartilage degradation and chondrocyte destruction, resulting in cartilage surface depressions, ulcers, joint deformities, and loss of joint function [35]. Generally, research on RA has focused on the impact of synovial hyperplasia on joints. Few reports have investigated cartilage, but recent studies have demonstrated that cartilage destruction occurs prior to arthritis. In 2012, the European League Against Rheumatism (EULAR) established different stages of pre-RA, shedding light on early or asymptomatic phases of the disease. Pre-RA is considered a "window of opportunity" [36] for treatment, emphasizing the importance of early intervention. Studies have revealed that pathological changes in bone and cartilage can be observed before the onset of synovitis in pre-RA. Patients often experience clinical symptoms such as bone pain, fatigue, joint discomfort, fever, and systemic malaise during this preclinical phase [37]. Comparative analyses between pre-RA and non-RA cohorts revealed strong correlations with TNFα and IL-1β [38]. Clinical data demonstrate that bone and cartilage loss occur before the onset of inflammation during the autoimmune phase. Early serological findings include positive anti-CII antibodies and alterations in the N-terminal peptide of type I procollagen (P1NP) [39]. Using a mouse CIA model, we found that mice exhibit a reduction in the extracellular matrix of articular cartilage, decreased collagen, increased osteoclasts, and weight loss before the onset of arthritis. These findings align with the pathological changes observed in human patients in the early clinical stages [40].

CIA is the most widely used animal model in RA research because of its similarities with RA, such as systemic chronic inflammation, synovial hyperplasia, mononuclear cell infiltration, cartilage degradation, and bone destruction. Like RA, CIA is associated with susceptibility and the expression of specific MHC class II genes [41]. However, the main differences are the absence of ACPAs and elevated RF levels in individuals with CIA, as well as the absence of notable sex differences and self-limiting inflammation. The CIA model involves two injections of CII on day 0 and day 14 or 21 to elicit a specific response from T and B cells, which mimics the effects of autoimmunity. Through control of the dosage of injection, the arthritis model can be manipulated, as the pathogenesis of CIA is largely mediated by CII-specific antibodies (predominantly the IgG2 subclass) that bind to and activate

(See figure on next page.)

Fig. 6 MVs protect chondrocytes. **a**–**c** Effects of MVs on chondrocyte migration (migration assay, ImageJ was used to measure the migratory distance and scratch blank area), proliferation (CCK-8 was used to detect proliferation, while red O staining was used to observe chondrocyte proliferation) and apoptosis (Annexin V-FITC/PI double staining, flow cytometry analysis, and Annexin V^+/PI^+ staining were used as indicators of apoptosis). **d**–**f** Effect of MVs on RNA expression in chondrocytes. After stimulation with MVs, whole-transcriptome analysis via total RNA sequencing (RNA-Seq) revealed 43 circRNAs, 101 miRNAs, and 45 lncRNAs in chondrocytes, as detailed in Table 3. **g**, **h** Effects of MVs on IL-1β- and TNFα-stimulated MMP-13 and ADAMTS-5 [immunofluorescence (red: MMP-13/ADAMTS-5; blue: DAPI) and RT-qPCR] in chondrocytes. **i**–**k** Effects of MVs on CI and CII in IL-1β- and TNFα-stimulated chondrocytes [immunofluorescence (CI-red, CII-green, and DAPI-blue and western blotting]. **l** Relationship between cartilage destruction and the IL-1β/TNFα/ADAMTS-5/MMP-13 ratio. The data are presented as the means ± SDs and were analyzed via one-way ANOVA followed by Tukey's post hoc tests. Two-tailed P values < 0.05 were considered significant

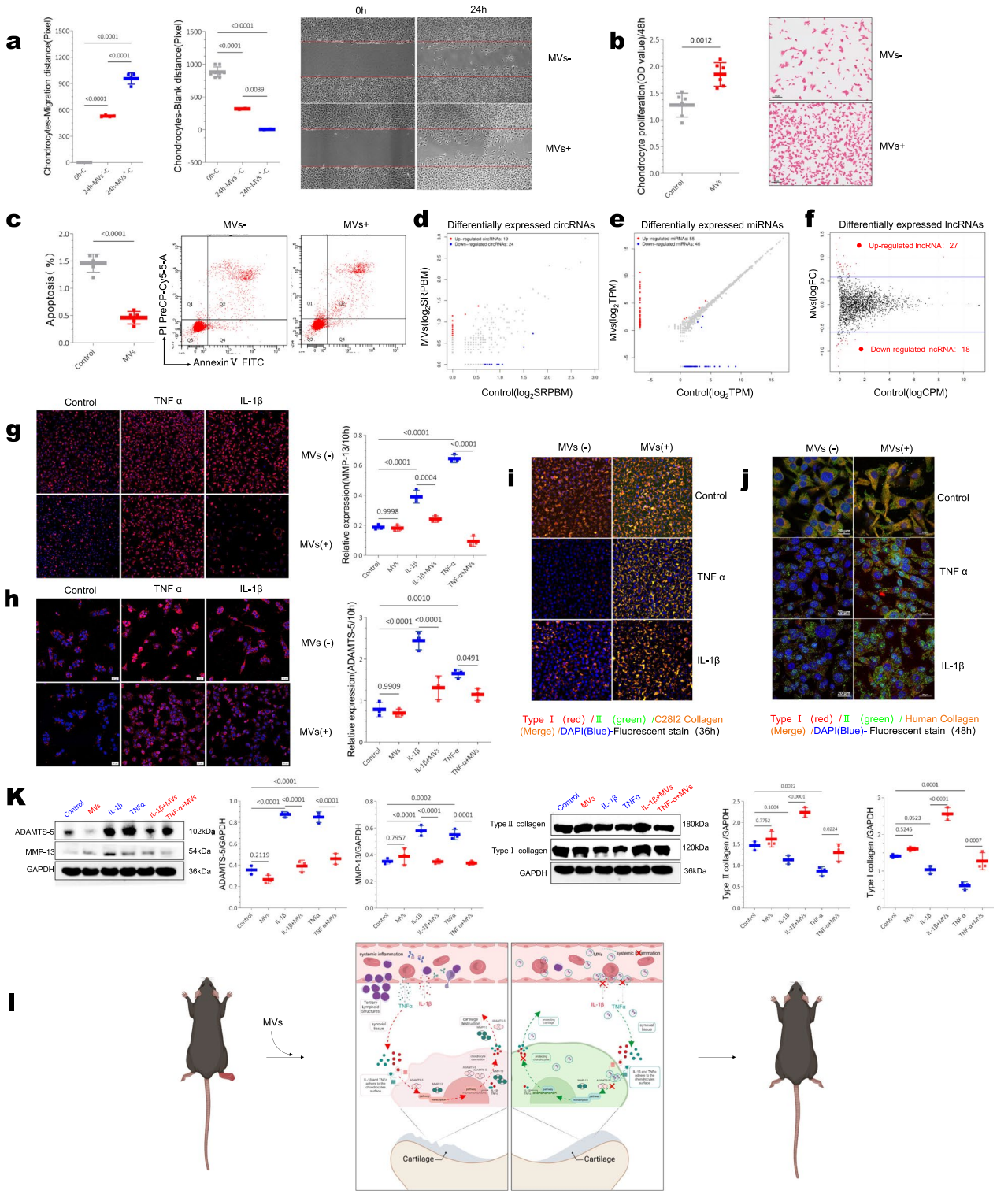

Fig. 6 (See legend on previous page.)

complement, leading to arthritis. The cellular cytokines and immune cells involved in early CIA closely reflect the majority of the pathological mechanisms underlying early RA immune alterations, including proinflammatory Th1 cells, anti-inflammatory Th2 cells, Th17 cells, follicular helper T (Tfh) cells assisting in B-cell activation

Table 3 hCartilage_MSCMVs-hCartilage_Control-differential gene/RNA expression

Gene			
Geneid	**hCartilage_MSCMVs**	**hCartilage_Control**	**PValue**
RGS16	**0.735741633**	0.350765332	0.00223791
ASB13	**0.639781401**	0.311142807	0.002455862
MTRNR2L8	**2.584698373**	0.87643731	2.49E−07
BCO2	**0.153151072**	0.070343603	0.009213888
SLC37A2	**0.202225197**	0.094513311	0.006559978
RP4-816N1.8	**0.910321958**	0.391430271	0.004809394
CCDC65	**0.742959057**	0.367497286	0.003652463
CDH24	**0.657347374**	0.321314996	0.000998205
SLC10A1	**1.400973045**	0.678946303	0.000547773
USP50	**0.320022923**	0.653285683	0.008150169
RBPMS2	0.387297296	0.800500394	0.003520526
HYKK	**0.301005019**	0.145530728	0.002909258
ZNF843	**0.475437698**	0.22292205	0.000940112
MTRNR2L1	**3.158321196**	1.042859329	8.41E−09
PSPN	**0.329423864**	0.143343674	0.003157896
ZNF726	0.089851727	0.293840054	3.72E−06
C2orf61	**0.414355647**	0.158597591	0.000658114
DERL3	0.160770209	0.328191728	0.008150169
LRRC75B	0.165130775	0.339790009	0.009865202
MTRNR2L12	**4.654213267**	1.425146766	1.07E−09
C3orf33	0.233021655	0.544874138	0.003161754
RP11-211G3.2	**1.264509121**	0.6170999	0.004642566
SLC27A6	**0.433555035**	0.202107726	0.002480876
SAMD5	**0.214586398**	0.098561376	0.004834217
ABCA13	0.03081056	0.097972302	4.98E−06
ADAM22	0.075967466	0.154888703	0.002455862
OPLAH	0.355394663	0.718237619	0.000489943
SPATA6L	**0.218016593**	0.104368031	0.002989694
TRPM3	**0.07378473**	0.035454112	0.003773522
TCEANC	**0.311111305**	0.130988088	0.000576244
MTRNR2L10	**8.450309483**	2.103501619	2.60E−16
CHRDL1	0.149918524	0.323106988	0.004597086
RP11-54O7.14	**2.530197822**	1.187966971	0.011720469
RP11-131M11.3	0.131108472	0.355293562	0.000588384
PRR13P1	1.440393662	3.104361261	0.004597086
LGALS8-AS1	0.372322864	0.840804531	0.003423805
LINC00704	**0.565077513**	0.227101838	0.002390599
BMS1P21	**3.344020354**	1.365277587	0.001920569
RP11-127L20.3	**1.70589438**	0.827061501	0.003378543
CTD-3236F5.1	**3.50737767**	0.930781918	5.42E−05
ST3GAL4-AS1	0.254990659	0.529825861	0.001920044
RP5-1057I20.6	**2.75968088**	1.086467266	0.000756638
RNA5SP370	**10.46093909**	4.118399332	0.001157928
RP11-545P7.4	3.463378308	6.949106937	0.004388966
WASF3-AS1	**0.49816044**	0.245884697	0.004823037
BNIP3P1	0.34225515	0.707403292	0.010890325
SNORD113-4	6.630242825	13.5655498	0.016842613
MIR1197	**13.09952418**	4.954949196	0.001065918

Table 3 (continued)

Gene			
Geneid	**hCartilage_MSCMVs**	**hCartilage_Control**	**PValue**
RP11-5N19.3	0.546448584	1.118039819	0.016842613
RP11-797A18.3	2.054827322	4.56169926	0.004334378
RP11-762H8.1	1.761934341	3.699527239	0.003132815
RP11-166B2.3	0.211667831	0.874987684	4.56E−06
RP11-1102P22.1	0.43911954	1.528608341	1.16E−05
SH3GL1P2	**1.378747353**	0.633270507	0.002156652
RP11-613C6.4	**3.179641055**	1.396939223	0.006193663
RP11-166P13.3	0.687345747	1.384239775	0.011137544
RP11-180P8.3	**1.536614291**	0.569177539	0.000395595
CTD-2265O21.7	**2.379273741**	1.138355078	0.012050518
RPL12P42	**5.118537798**	2.413404017	0.000445635
RP11-474G23.3	**1.108221477**	0.466597677	0.003725415
CACYBPP2	1.800246946	3.889346272	0.000406958
RP5-1009E24.8	**1.287009283**	0.566503823	0.005648832
RPL24P2	0.856538547	2.273067421	0.001489598
MIR3648-1	**115.7781039**	48.33303882	1.79E−08
CH507-513H4.6	**1.15097045**	0.517402733	0.007223709
CH507-513H4.5	**2598.107637**	1261.652821	4.55E−07
CH507-513H4.4	**1.81216624**	0.67487313	9.99E−05
CH507-513H4.3	**182.9798128**	82.64946265	3.97E−08
CTA-221G9.12	0.472374097	1.301792892	0.000448896
CTA-223H9.9	**2.301220643**	0.986505722	0.00525818
AL022476.2	0.162768367	0.598087277	2.43E−05
RP11-415F23.3	**2.284355906**	1.104446629	0.009186286
RPL29P11	0.872883964	2.532145931	0.000267908
RNA5SP131	**9.87698511**	2.093808064	1.95E−06
RP11-381E24.1	0.9769513	1.998853114	0.016842613
SEPSECS-AS1	**0.243881021**	0.119166647	0.015130572
LINC01094	0.168508374	0.422167332	0.001157928
RP11-455G16.1	**0.413135469**	0.185539856	0.007955833
RP11-1336O20.2	0.245574655	0.516975018	0.008680466
CTD-2325A15.5	0.898136445	1.856348043	0.010890325
CTC-351M12.1	0.262996645	0.597272172	0.000739546
GUSBP9	**1.780381207**	0.817744388	0.009213888
MIR5690	**17.64899631**	7.679686425	0.003157896
BTBD9-AS1	0.403626795	1.853892556	1.72E−05
RP11-134K13.2	0.451651419	1.093813447	0.001920569
RNA5SP216	**58.98857946**	17.72502151	3.06E−11
AC002480.3	**0.483289979**	0.239054566	0.01381579
RP11-274B21.3	0.749439673	1.542123888	0.009865202
RNA5SP248	**130.101311**	62.12729701	2.37E−06
RP11-111F5.5	0.197406992	0.397556267	0.011137544
RP11-62C3.6	1.493297934	3.055304009	0.016842613
MT-RNR1	**301.9906913**	130.5451285	6.30E−09
MT-RNR2	**1069.08751**	372.5860268	3.46E−13
RNA5SP506	**33.42979576**	14.30768843	1.38E−05
DDX3P1	0.231826672	0.521751915	0.007955833
RP1-203P18.1	**1.304025031**	0.630473582	0.009186286

Table 3 (continued)

Gene			
Geneid	**hCartilage_MSCMVs**	**hCartilage_Control**	**PValue**
AC010970.2	**4.146347989**	1.46064262	3.03E−09
miRNA			
miRNA	**hCartilage_MSCMVs**	**hCartilage_Control**	**PValue**
novel_163	**1598.807795**	0	4.27E−163
novel_164	**478.168783**	0	5.34E−113
novel_208	**350.4606335**	0	1.14E−100
novel_165	**281.6947068**	0	3.23E−92
novel_166	**210.2272616**	0	3.11E−81
novel_210	**126.7257792**	0	2.78E−65
novel_167	**62.3805192**	0	1.28E−43
novel_168	**47.15377829**	0	1.82E−36
hsa-miR-549a	**43.22429677**	17.81641041	9.67E−06
novel_170	**33.89177815**	0	5.55E−29
novel_169	**17.43707427**	0	1.46E−17
hsa-miR-548e-3p	**17.19148167**	8.520891936	0.007163685
novel_206	**16.70029648**	0	5.94E−17
novel_171	**12.77081495**	0	1.49E−13
novel_176	**10.80607419**	0	9.60E−12
novel_172	**10.314889**	0	2.80E−11
novel_173	**7.367777859**	0	2.21E−08
novel_199	**6.631000073**	0	1.26E−07
novel_217	**5.648629692**	0	7.45E−07
novel_207	**5.403037096**	0	1.36E−06
hsa-miR-3199	**4.911851906**	2.065670772	0.048953034
hsa-miR-3130-3p	**4.420666715**	1.549253079	0.031052599
novel_202	**4.420666715**	0	1.54E−05
novel_220	**4.17507412**	0	2.86E−05
novel_177	**4.17507412**	0	2.86E−05
novel_178	**3.683888929**	0	9.96E−05
novel_209	**3.438296334**	0	0.000187
novel_205	**3.438296334**	0	0.000187
novel_221	**3.438296334**	0	0.000187
novel_201	**3.438296334**	0	0.000187
novel_175	**3.192703739**	0	0.000352487
novel_197	**2.947111143**	0	0.000667207
novel_218	**2.947111143**	0	0.000667207
novel_204	**2.947111143**	0	0.000667207
novel_180	**2.947111143**	0	0.000667207
novel_219	**2.701518548**	0	0.001268294
novel_211	**2.701518548**	0	0.001268294
novel_174	**2.701518548**	0	0.001268294
novel_215	**2.701518548**	0	0.001268294
novel_216	**2.455925953**	0	0.002421289
novel_228	**2.210333358**	0	0.004642655
novel_226	**2.210333358**	0	0.004642655
novel_179	**2.210333358**	0	0.004642655
novel_181	**2.210333358**	0	0.004642655

Table 3 (continued)

miRNA			
miRNA	**hCartilage_MSCMVs**	**hCartilage_Control**	**PValue**
novel_222	**2.210333358**	0	0.004642655
novel_224	**1.964740762**	0	0.00894141
novel_227	**1.964740762**	0	0.00894141
novel_183	**1.964740762**	0	0.00894141
novel_182	**1.964740762**	0	0.00894141
novel_223	**1.964740762**	0	0.00894141
novel_225	**1.964740762**	0	0.00894141
novel_186	**1.719148167**	0	0.017297867
novel_185	**1.719148167**	0	0.017297867
hsa-miR-6505-5p	**1.719148167**	0	0.017297867
novel_187	**1.473555572**	0	0.03361661
hsa-miR-320d	5.894222287	12.91044233	0.006572989
hsa-miR-378d	2.947111143	7.229847703	0.021118495
hsa-miR-122-5p	1.473555572	11.36118925	3.66E−07
novel_2	0	546.3699193	2.80E−120
novel_10	0	240.650645	5.06E−88
novel_21	0	87.27459013	3.14E−53
novel_22	0	50.35072508	7.19E−38
novel_31	0	28.91939081	1.30E−25
novel_123	0	23.75521388	3.86E−22
novel_30	0	19.62387234	3.83E−19
novel_34	0	16.78357503	9.51E−17
novel_42	0	8.779100783	7.43E−10
novel_116	0	6.71343001	1.26E−07
novel_50	0	5.938803471	7.45E−07
novel_148	0	5.680594624	1.36E−06
novel_47	0	5.680594624	1.36E−06
novel_91	0	4.905968084	8.35E−06
novel_52	0	4.647759238	1.54E−05
novel_120	0	4.131341545	5.33E−05
novel_83	0	3.614923852	0.000187
novel_48	0	3.356715005	0.000352487
novel_127	0	3.356715005	0.000352487
novel_97	0	3.356715005	0.000352487
novel_89	0	3.098506159	0.000667207
novel_54	0	3.098506159	0.000667207
novel_145	0	3.098506159	0.000667207
novel_56	0	3.098506159	0.000667207
novel_84	0	3.098506159	0.000667207
novel_96	0	3.098506159	0.000667207
novel_142	0	2.840297312	0.001268294
novel_70	0	2.840297312	0.001268294
novel_61	0	2.582088465	0.002421289
novel_136	0	2.582088465	0.002421289
hsa-miR-545-5p	0	2.582088465	0.002421289
novel_151	0	2.323879619	0.004642655
novel_156	0	2.323879619	0.004642655
novel_149	0	2.323879619	0.004642655

Table 3 (continued)

miRNA			
miRNA	**hCartilage_MSCMVs**	**hCartilage_Control**	**PValue**
novel_64	0	2.065670772	0.00894141
novel_158	0	2.065670772	0.00894141
hsa-miR-548i	0	2.065670772	0.00894141
novel_159	0	1.807461926	0.017297867
novel_62	0	1.807461926	0.017297867
novel_155	0	1.807461926	0.017297867
novel_161	0	1.807461926	0.017297867
novel_65	0	1.549253079	0.03361661
novel_67	0	1.549253079	0.03361661
lncRNA			
Geneid	**hCartilage_MSCMVs**	**hCartilage_Control**	**PValue**
RP11-12G12.7	0.618923892	1.137108249	0.035679272
RP11-1114A5.4	**0.374471513**	0.199517661	0.028529249
AC108488.4	**1.121302638**	0.664109814	0.029508817
AC092614.2	**1.317892551**	0.753793937	0.036837517
C2orf48	0.417031375	0.711456922	0.047331031
RP11-452F19.3	**1.374370005**	0.815782094	0.035179146
LINC01094	0.168508374	0.422167332	0.001157928
CTD-2349P21.6	**2.849956155**	1.624977128	0.032273079
MIR193BHG	0.535849366	0.924815367	0.041412271
RP11-166P13.3	0.687345747	1.384239775	0.011137544
LINC01021	0.36843568	0.629676926	0.025967455
RP11-648L3.2	**1.6635882**	0.896987374	0.035679272
LINC01515	0.225018422	0.12815759	0.009866245
AP006621.5	1.643473788	2.764558192	0.011742982
RP11-127L20.3	**1.70589438**	0.827061501	0.003378543
AC112721.1	1.345422651	2.259983307	0.047331031
RP5-1009E24.8	**1.287009283**	0.566503823	0.005648832
OSER1-AS1	0.310198086	0.607900359	0.012733234
RP11-180P8.3	**1.536614291**	0.569177539	0.000395595
RP11-111M22.3	**2.548094888**	1.431972181	0.014593386
RP11-797A18.3	2.054827322	4.56169926	0.004334378
RP11-14N7.2	1.266204679	2.276818701	0.011639837
KCCAT211	**1.053056265**	0.573503667	0.002254381
LINC00571	**1.662273666**	1.05309873	0.038728298
RP11-111F5.4	0.392154199	0.674491142	0.01841685
AC092171.4	1.112425742	1.673350451	0.020186389
LINC00704	**0.565077513**	0.227101838	0.002390599
TCONS_00037359	**2.89382256**	1.580619813	0.012781993
TCONS_00108246	**2.80081898**	1.534700621	0.022754965
TCONS_00100001	1.496186324	2.699758427	0.031199551
TCONS_00033771	0.725491815	1.19960865	0.03424284
TCONS_00001919	0.804858179	1.509519636	0.032492464
TCONS_00045940	0.504599749	0.899801299	0.031449559
TCONS_00119646	**36.96680456**	18.22507182	8.31E−07
TCONS_00062215	**2.685516896**	1.603525284	0.047331031
TCONS_00057831	**1.321116397**	0.728160137	0.025220408

Table 3 (continued)

lncRNA			
Geneid	**hCartilage_MSCMVs**	**hCartilage_Control**	**PValue**
TCONS_00103307	**1.134230105**	0.723731133	0.045614707
TCONS_00068379	**1.770122331**	1.011078752	0.017416768
TCONS_00035579	**1.735918121**	0.963430884	0.042394422
TCONS_00065096	**1.932607109**	0.926257099	0.013367305
TCONS_00071099	0.639040539	1.152325258	0.034829425
TCONS_00014297	**2.754343006**	1.686791216	0.048474458
TCONS_00035175	**3.526724907**	2.012547191	0.023507193
TCONS_00003331	**1.576960503**	0.877953346	0.018282338
TCONS_00047885	**1.348674428**	0.852081131	0.027512072
CircRNA			
ID	**hCartilage_MSCMVs**	**hCartilage_Control**	**PValue**
22:50372019–50394135	0	0.611553337	0.03361661
1:59339957–59378837	0	0.917330006	0.004642655
3:27448650–27452498	0	0.764441672	0.017297867
3:56592969–56594028	0	0.713478893	0.017297867
3:169976945–169988359	0	0.662516115	0.03361661
3:172247532–172251541	0	0.764441672	0.017297867
3:196487398–196488683	**1.25822457**	0.203851112	0.016084066
2:201145377–201149835	0	0.662516115	0.03361661
2:214767481–214781509	0	0.611553337	0.03361661
5:83537006–83555038	0	0.662516115	0.03361661
5:123545416–123557564	0	0.611553337	0.03361661
4:87046165–87047594	0.328232496	1.834660012	0.003944816
7:18666212–18666476	0	0.764441672	0.017297867
7:92294888–92327900	0	0.611553337	0.03361661
6:72295936–72333835	0	0.968292784	0.004642655
9:5968018–5988545	**1.586457066**	0.458665003	0.025042572
8:67131950–67137603	0	0.764441672	0.017297867
10:67954594–68014186	0	0.764441672	0.017297867
10:67966682–68014186	0	1.07021834	0.002421289
13:32517856–32527532	0.656464993	2.242362236	0.009625718
15:75859877–75873568	0	0.611553337	0.03361661
15:93000511–93014909	0	0.662516115	0.03361661
17:16101249–16101805	0	0.611553337	0.03361661
17:45081643–45086652	0	0.662516115	0.03361661
16:16111374–16111582	0	0.611553337	0.03361661
18:21765771–21819646	0	0.764441672	0.017297867
1:27789561–27793632	**0.765875825**	0	0.017297867
1:28742402–28743986	**0.820581241**	0	0.00894141
2:36396613–36442735	**0.601759577**	0	0.03361661
2:63856305–63857936	**0.656464993**	0	0.03361661
5:14330777–14336727	**0.929992073**	0	0.004642655
4:2699679–2700544	**0.601759577**	0	0.03361661
4:2949933–2953645	**0.601759577**	0	0.03361661
7:156826604–156836885	**0.601759577**	0	0.03361661
6:56851396–56900621	**0.601759577**	0	0.03361661
9:37424844–37426654	**0.711170409**	0	0.017297867

Table 3 (continued)

CircRNA			
ID	**hCartilage_MSCMVs**	**hCartilage_Control**	**PValue**
Y:2953908–2961646	**0.601759577**	0	0.03361661
12:122340752–122341697	**0.929992073**	0	0.004642655
15:44328684–44380976	**1.203519153**	0	0.001268294
17:77402058–77402703	**1.039402905**	0	0.002421289
17:82563353–82568201	**0.875286657**	0	0.00894141
19:34430575–34434968	**0.601759577**	0	0.03361661
18:32111753–32113860	**0.656464993**	0	0.03361661

Bold—up; unbold—down

and antibody production, and the production of numerous inflammatory factors [42, 43]. Thus, the CIA model is suitable for studying early or pre-RA. In our study, we also observed changes in immune cells, inflammatory cytokines, and cartilage following the injection of the collagen emulsion in the early stage, which was consistent with clinical symptoms and characteristics.

RA is estimated to affect 0.5–1% of the total population, resulting in a major burden on society because of the need for long-term treatment and working years of life lost. Despite advancements in RA treatment and the introduction of disease-modifying rheumatoid arthritis drugs (DMARDs), many patients suffer from refractory RA, and the long-term side effects of medication pose serious risks to their health [44–46]. Therefore, more attention has been given to the early stages of the disease as a "window of opportunity" for treatment, as therapy at this stage may change the course of disease development. This notion has been supported by research on early or preclinical stages of RA, where studies on stem cells [47], biologics (abatacept [48], tocilizumab [49]), and antirheumatic drugs [50] have been conducted and showed that earlier treatment leads to long-term benefits for patients. The 2010 Rheumatoid Arthritis Classification Criteria: an American College of Rheumatology/European League Against Rheumatism (ACR/EULAR) collaborative initiative has also promoted early diagnosis and treatment. Cartilage invasion represents irreversible destruction, and chronic inflammation following the onset of RA also appears to be irreversible. Therefore, treatments administered during preclinical stages where pathological changes are still reversible could be crucial. Stem cell research has shown that stem cells can alleviate the symptoms of RA patients through immunomodulation and cartilage regeneration, playing an important role in refractory RA [51]. In a study of stem cell-derived extracellular vesicles and MVs, these vesicles were found to have important immunomodulatory effects on RA [52]. In our study, after intravenous injection of MVs in CIA model mice, MVs seemed to accumulate in immune organs and inflamed areas. Additionally, mice with CIA presented significant improvements in joint scores and inflammation, as well as a reduction in articular cartilage changes. Early intervention may have the potential to alter the outcome of this disease.

In arthritis, cartilage destruction is the direct cause of joint dysfunction. The mechanisms underlying cartilage destruction in arthritis are complex and involve factors such as inflammation, abnormal cartilage cell function, enzyme activation, and the involvement of inflammatory cytokines [53, 54]. From a pathological perspective, cartilage degradation and matrix degradation are the core processes of arthritis-related cartilage destruction [55]. Previous studies have shown that TNFα and IL-1β can directly damage cartilage cells and promote other destructive mechanisms [56]. TNFα can exert a direct toxic effect on cartilage cells, leading to their apoptosis. Moreover, TNFα can stimulate the production of other inflammatory cytokines and enzymes, such as IL-1β, IL-6, and matrix metalloproteinases (MMPs), by cartilage cells, further exacerbating the process of arthritis [57]. IL-1β primarily promotes inflammatory responses and tissue damage. This molecule directly stimulates cartilage cells to produce enzymes, such as MMPs and aggrecanases (AGGs), leading to the degradation and destruction of the cartilage matrix. TNFα and IL-1β can also induce the production of ADAMTSs (ADAMTS-4 and ADAMTS-5) by cartilage cells and other cells. ADAMTSs are capable of cleaving and degrading specific molecules in cartilage tissue, such as proteoglycans and collagen [58]. Overactivation of ADAMTSs leads to the degradation of aggrecan molecules, which in turn results in the destruction and loss of the cartilage matrix, thereby affecting the structure and function of cartilage. In this study, both in vitro and in vivo experiments confirmed that MVs can reduce TNFα and IL-1β levels, thereby decreasing the levels of

MMPs and ADAMTSs and improving joint conditions. Notably, IL-6 appears to be more abundant in the synovium and less prevalent in cartilage tissue.

In summary, MSCs-MVs possess the characteristics of MSCs and exert a protective effect on the joints of mice with CIA. However, the therapeutic effects of MVs remain complex, and the specific mechanisms underlying their effects are difficult to ascertain. Nevertheless, MVs represent a promising new approach for the management of early RA. It is hoped that the "window of opportunity" for treating RA can be seized to reverse early damage and alter the disease course.

Conclusions

Injection of MSCs-MVs into early CIA models effectively controlled CIA, reducing cartilage destruction in the joints. The expression of IL-1β and TNFα in the serum and cartilage decreased, along with decreased expression of MMP-13 and ADAMTS-5 in the cartilage and reduced collagen content. In vitro experiments also confirmed that MVs can reduce IL-1β and TNFα expression in cartilage cells, thereby reducing the expression of MMP-13 and ADAMTS-5 and maintaining collagen expression in cartilage cells.

Abbreviations

pre-RA	Preclinical rheumatoid arthritis
MSC	Mesenchymal stem cell
MVs	Microvesicles
CIA	Collagen-induced arthritis
ELISAs	Enzyme-linked immunosorbent assays
PBMCs	Peripheral blood mononuclear cells
RA	Rheumatoid arthritis
ACR	The American College of Rheumatology
ACPA	Anti-cyclic citrullinated peptide antibody
anti-CII	Anti-collagen type II
RF	Rheumatoid factor
MRI	Magnetic resonance imaging
Exos	Exosomes
FBS	Fetal bovine serum
TEM	Transmission electron microscopy
micro-CT	Microcomputed tomography
H&E	Hematoxylin and eosin
TRAP	Tartrate-resistant acid phosphatase
RT-qPCR	Quantitative real-time PCR
RIPA	Radioimmunoprecipitation assay
LPS	Lipopolysaccharide
Tfh	Follicular helper T
DMARDs	Disease-modifying rheumatoid arthritis drugs
EULAR	European League Against Rheumatism
MMPs	Matrix metalloproteinases

Supplementary Information

The online version contains supplementary material available at https://doi.org/10.1186/s12951-024-02922-6.

Supplementary Material 1.

Acknowledgements

We thank Chengdu Kangjing Biotechnology Co., Ltd. (Chengdu Cell Bank) for providing mesenchymal stem cells and for providing technical and equipment support to the public experimental platform of Tianfu Life Science Park, West China Hospital of Sichuan University.

Author contributions

Professor Yi Liu, Xiao feng Zeng and Xinping Tian designed the experiments, ShixiongWei, Ruijuan Cheng and Sujia Li completed the main parts of the experiments, and Qiuping Zhang, Chen yang Lu, Qiu hong Wu and Xue ting Zhao participated in this research project.

Funding

This work was supported by Sichuan University West China Hospital Science and Technology Achievement Transformation Fund Project (CGZH21005) to Yi Liu, the Natural Science Foundation of Sichuan Province (Project No. 2023NSFSC1752) to Rui-Juan Cheng, and the Chinese National Key Technology R&D Program, Ministry of Science and Technology (2022YFC250460 , CAMS Innovation Fund for Medical Sciences (CIFMS) (2021-I2M-1-005, 2022-I2M-1-004, 2023-I2M-2-005), The Non-profit Central Research Institute Fund of Chinese Academy of Medical Sciences (2021-PT320-002, 2019-PT330-004), National High Level Hospital Clinical Research Funding (2022-PUMCH-B-013)

Availability of data and materials

No datasets were generated or analysed during the current study.

Declarations

Ethics approval and consent to participate

All procedures involving MSC-MVs to protect cartilage from degradation in early rheumatoid arthritis via immunoregulation were approved by the Animal Research Committee of West China Hospital, Sichuan University (Approval Number: 2020285A, Date of Approval: September 22, 2020), and the Research Committee of West China Hospital, Sichuan University for human participants (Approval Number: 1771, Date: December 22, 2022).

Consent for publication

Not applicable.

Competing interests

The authors declare no competing interests.

Author details

[1]Department of Rheumatology and Clinical Immunology, Peking Union Medical College Hospital, Chinese Academy of Medical Sciences, Peking Union Medical College. National Clinical Research Center for Dermatologic and Immunologic Diseases (NCRC-DID), Ministry of Science & Technology. State Key Laboratory of Complex Severe and Rare Diseases, Peking Union Medical College Hospital. Key Laboratory of Rheumatology and Clinical Immunology, Ministry of Education, Beijing 100730, China. [2]Department of Rheumatology and Immunology, West China Hospital, Sichuan University, Chengdu 610041, Sichuan, China.

Received: 26 May 2024 Accepted: 10 October 2024
Published online: 04 November 2024

References

1. Finckh A, Gilbert B, Hodkinson B, Bae SC, Thomas R, Deane KD, et al. Global epidemiology of rheumatoid arthritis. Nat Rev Rheumatol. 2022;18:591–602.
2. Wu D, Luo Y, Li T, Zhao X, Lv T, Fang G, et al. Systemic complications of rheumatoid arthritis: focus on pathogenesis and treatment. Front Immunol. 2022;13:1051082.
3. de Moel EC, Trouw LA, Terao C, Govind N, Tikly M, El-Gabalawy H, et al. Geo-epidemiology of autoantibodies in rheumatoid arthritis: comparison between four ethnically diverse populations. Arthritis Res Ther. 2023;25:37.

4. Kay J, Upchurch KS. ACR/EULAR 2010 rheumatoid arthritis classification criteria. Rheumatology. 2012;51:vi5–9.
5. Aletaha D, Neogi T, Silman AJ, Funovits J, Felson DT, Bingham CO, et al. 2010 Rheumatoid arthritis classification criteria: an American college of rheumatology/European league against rheumatism collaborative initiative. Arthritis Rheum. 2010;62:2569–81.
6. Arnett FC, Edworthy SM, Bloch DA, McShane DJ, Fries JF, Cooper NS, et al. The American rheumatism association 1987 revised criteria for the classification of rheumatoid arthritis. Arthritis Rheum. 1988;31:315–24.
7. Aletaha D, Smolen JS. Diagnosis and management of rheumatoid arthritis. JAMA. 2018;320:1360.
8. Cush JJ. Rheumatoid arthritis. Med Clin N Am. 2021;105:355–65.
9. Greenblatt HK, Kim HA, Bettner LF, Deane KD. Preclinical rheumatoid arthritis and rheumatoid arthritis prevention. Curr Opin Rheumatol. 2020;32:289–96.
10. Tracy A, Buckley CD, Raza K. Pre-symptomatic autoimmunity in rheumatoid arthritis: when does the disease start? Semin Immunopathol. 2017;39:423–35.
11. Lingampalli N, Sokolove J, Lahey LJ, Edison JD, Gilliland WR, Holers VM, et al. Combination of anti-citrullinated protein antibodies and rheumatoid factor is associated with increased systemic inflammatory mediators and more rapid progression from preclinical to clinical rheumatoid arthritis. Clin Immunol. 2018;195:119–26.
12. Verheul MK, Böhringer S, van Delft MAM, Jones JD, Rigby WFC, Gan RW, et al. Triple positivity for anti-citrullinated protein autoantibodies, rheumatoid factor, and anti-carbamylated protein antibodies conferring high specificity for rheumatoid arthritis. Arthritis Rheumatol. 2018;70:1721–31.
13. Bas DB, Su J, Sandor K, Agalave NM, Lundberg J, Codeluppi S, et al. Collagen antibody-induced arthritis evokes persistent pain with spinal glial involvement and transient prostaglandin dependency. Arthritis Rheumatol. 2012;64:3886–96.
14. Nandakumar KS, Bajtner E, Hill L, Böhm B, Rowley MJ, Burkhardt H, et al. Arthritogenic antibodies specific for a major type II collagen triple-helical epitope bind and destabilize cartilage independent of inflammation. Arthritis Rheumatol. 2007;58:184–96.
15. de Hair MJH, van de Sande MGH, Ramwadhdoebe TH, Hansson M, Landewé R, van der Leij C, et al. Features of the synovium of individuals at risk of developing rheumatoid arthritis: implications for understanding preclinical rheumatoid arthritis. Arthritis Rheumatol. 2014;66:513–22.
16. Ge L, Fu Z, Wei Y, Shi D, Geng Y, Fan H, et al. Preclinical evaluation and pilot clinical study of [18F]AlF-NOTA-FAPI-04 for PET imaging of rheumatoid arthritis. Eur J Nucl Med Mol Imaging. 2022;49:4025–36.
17. De Jong TA, de Hair MJH, van de Sande MGH, Semmelink JF, Choi IY, Gerlag DM, et al. Synovial gene signatures associated with the development of rheumatoid arthritis in at risk individuals: a prospective study. J Autoimmun. 2022;133: 102923.
18. Martins P, Fonseca JE. How to investigate: pre-clinical rheumatoid arthritis. Best Pract Res Clin Rheumatol. 2019;33: 101438.
19. van Steenbergen HW, van Nies JAB, Huizinga TWJ, Reijnierse M, van der Helm-Van Mil AHM. Subclinical inflammation on MRI of hand and foot of anticitrullinated peptide antibody-negative arthralgia patients at risk for rheumatoid arthritis. Arthritis Res Ther. 2014;16:R92.
20. Berntson L, Nordal E, Fasth A, Aalto K, Herlin T, Nielsen S, et al. Anti-type II collagen antibodies, anti-CCP, IgA RF and IgM RF are associated with joint damage, assessed eight years after onset of juvenile idiopathic arthritis (JIA). Pediatr Rheumatol. 2014;12:22.
21. Watanabe Y, Tsuchiya A, Terai S. The development of mesenchymal stem cell therapy in the present, and the perspective of cell-free therapy in the future. Clin Mol Hepatol. 2021;27:70–80.
22. Wang LT, Liu KJ, Sytwu HK, Yen ML, Yen BL. Advances in mesenchymal stem cell therapy for immune and inflammatory diseases: use of cell-free products and human pluripotent stem cell-derived mesenchymal stem cells. Stem cells Transl Med. 2021;10:1288–303.
23. Vizoso FJ, Eiro N, Cid S, Schneider J, Perez-Fernandez R. Mesenchymal stem cell secretome: toward cell-free therapeutic strategies in regenerative medicine. Int J Mol Sci. 2017;18:1852.
24. Kumar P, Kandoi S, Misra R, Vijayalakshmi S, Rajagopal K, Verma RS. The mesenchymal stem cell secretome: a new paradigm towards cell-free therapeutic mode in regenerative medicine. Cytokine Growth Factor Rev. 2019;46:1–9.
25. Shen Z, Huang W, Liu J, Tian J, Wang S, Rui K. Effects of mesenchymal stem cell-derived exosomes on autoimmune diseases. Front Immunol. 2021;12: 749192.
26. Vizoso FJ, Eiro N, Costa L, Esparza P, Landin M, Diaz-Rodriguez P, et al. Mesenchymal stem cells in homeostasis and systemic diseases: hypothesis, evidences, and therapeutic opportunities. Int J Mol Sci. 2019;20:3738.
27. Cosenza S, Ruiz M, Toupet K, Jorgensen C, Noël D. Mesenchymal stem cells derived exosomes and microparticles protect cartilage and bone from degradation in osteoarthritis. Sci Rep. 2017;7:16214.
28. Najar M, Melki R, Khalife F, Lagneaux L, Bouhtit F, Moussa Agha D, et al. Therapeutic mesenchymal stem/stromal cells: value, challenges and optimization. Front Cell Dev Biol. 2022;9: 716853.
29. Mishra VK, Shih HH, Parveen F, Lenzen D, Ito E, Chan TF, et al. Identifying the therapeutic significance of mesenchymal stem cells. Cells. 2020;9:1145.
30. Lovell-Badge R, Anthony E, Barker RA, Bubela T, Brivanlou AH, Carpenter M, et al. ISSCR guidelines for stem cell research and clinical translation: the 2021 update. Stem Cell Rep. 2021;16:1398–408.
31. Xunian Z, Kalluri R. Biology and therapeutic potential of mesenchymal stem cell-derived exosomes. Cancer Sci. 2020;111:3100–10.
32. Han Y, Yang J, Fang J, Zhou Y, Candi E, Wang J, et al. The secretion profile of mesenchymal stem cells and potential applications in treating human diseases. Sig Transduct Target Ther. 2022;7:92.
33. Mendt M, Rezvani K, Shpall E. Mesenchymal stem cell-derived exosomes for clinical use. Bone Marrow Transplant. 2019;54:789–92.
34. Haraszti RA, Didiot MC, Sapp E, Leszyk J, Shaffer SA, Rockwell HE, et al. High-resolution proteomic and lipidomic analysis of exosomes and microvesicles from different cell sources. J Extracell Vesicles. 2016;5:32570.
35. Komatsu N, Takayanagi H. Mechanisms of joint destruction in rheumatoid arthritis—immune cell–fibroblast–bone interactions. Nat Rev Rheumatol. 2022;18:415–29.
36. Resman-Targoff BH, Cicero MP. Aggressive treatment of early rheumatoid arthritis: recognizing the window of opportunity and treating to target goals. Am J Manag Care. 2010;16:S249–58.
37. Ramwadhdoebe TH, Hähnlein J, Maijer KI, van Boven LJ, Gerlag DM, Tak PP, et al. Lymph node biopsy analysis reveals an altered immunoregulatory balance already during the at-risk phase of autoantibody positive rheumatoid arthritis. Eur J Immunol. 2016;46:2812–21.
38. Sokolove J, Bromberg R, Deane KD, Lahey LJ, Derber LA, Chandra PE, et al. Autoantibody epitope spreading in the pre-clinical phase predicts progression to rheumatoid arthritis. PLoS ONE. 2012;7: e35296.
39. Mullazehi M, Wick MC, Klareskog L, van Vollenhoven R, Rönnelid J. Anti-type II collagen antibodies are associated with early radiographic destruction in rheumatoid arthritis. Arthritis Res Ther. 2012;14:R100.
40. Raza K, Holers VM, Gerlag D. Nomenclature for the phases of the development of rheumatoid arthritis. Clin Ther. 2019;41:1279–85.
41. Brand DD, Latham KA, Rosloniec EF. Collagen-induced arthritis. Nat Protoc. 2007;2:1269–75.
42. Rosloniec EF, Cremer M, Kang AH, Myers LK, Brand DD. Collagen-induced arthritis. Curr Protoc Immunol. 2010;89:15.5. 1–25.
43. Cho YG, Cho ML, Min SY, Kim HY. Type II collagen autoimmunity in a mouse model of human rheumatoid arthritis. Autoimmun Rev. 2007;7:65–70.
44. van der Woude D, van der Helm-Van Mil AHM. Update on the epidemiology, risk factors, and disease outcomes of rheumatoid arthritis. Best Pract Res Clin Rheumatol. 2018;32:174–87.
45. Sidiropoulos P, Bounas A, Galanopoulos N, Vosvotekas G, Koukli EM, Georgiou P, et al. Treatment satisfaction, patient preferences, and the impact of suboptimal disease control in rheumatoid arthritis patients in Greece: analysis of the Greek cohort of SENSE study. Mediterr J Rheumatol. 2022;33:14–34.
46. Conigliaro P, Triggianese P, De Martino E, Fonti GL, Chimenti MS, Sunzini F, et al. Challenges in the treatment of rheumatoid arthritis. Autoimmun Rev. 2019;18:706–13.
47. Harna B, Kalra P, Arya S, Jeyaraman N, Nallakumarasamy A, Jeyaraman M, et al. Mesenchymal stromal cell therapy for patients with rheumatoid arthritis. Exp Cell Res. 2023;423: 113468.
48. Al-Laith M, Jasenecova M, Abraham S, Bosworth A, Bruce IN, Buckley CD, et al. Arthritis prevention in the pre-clinical phase of RA with abatacept (the APIPPRA study): a multi-centre, randomised, double-blind, parallel-group, placebo-controlled clinical trial protocol. Trials. 2019;20:429.

49. Gerlag DM, Safy M, Maijer KI, Tang MW, Tas SW, Starmans-Kool MJF, et al. Effects of B-cell directed therapy on the preclinical stage of rheumatoid arthritis: the PRAIRI study. Ann Rheum Dis. 2019;78:179–85.
50. Teitsma XM, Jacobs JWG, Welsing PMJ, Pethö-Schramm A, Borm MEA, van Laar JM, et al. Radiographic joint damage in early rheumatoid arthritis patients: comparing tocilizumab- and methotrexate-based treat-to-target strategies. Rheumatology. 2017;57:309–17.
51. Ghoryani M, Shariati-Sarabi Z, Tavakkol-Afshari J, Ghasemi A, Poursamimi J, Mohammadi M. Amelioration of clinical symptoms of patients with refractory rheumatoid arthritis following treatment with autologous bone marrow-derived mesenchymal stem cells: a successful clinical trial in Iran. Biomed Pharmacother. 2019;109:1834–40.
52. Heydari R, Koohi F, Rasouli M, Rezaei K, Abbasgholinejad E, Bekeschus S, et al. Exosomes as rheumatoid arthritis diagnostic biomarkers and therapeutic agents. Vaccines. 2023;11:687.
53. Tateiwa D, Yoshikawa H, Kaito T. Cartilage and bone destruction in arthritis: pathogenesis and treatment strategy: a literature review. Cells. 2019;8:818.
54. Goldring SR. Pathogenesis of bone and cartilage destruction in rheumatoid arthritis. Rheumatology. 2003;42:ii11–6.
55. Tseng CC, Chen YJ, Chang WA, Tsai WC, Ou TT, Wu CC, et al. Dual role of chondrocytes in rheumatoid arthritis: the chicken and the egg. Int J Mol Sci. 2020;21:1071.
56. Kapoor M, Martel-Pelletier J, Lajeunesse D, Pelletier JP, Fahmi H. Role of proinflammatory cytokines in the pathophysiology of osteoarthritis. Nat Rev Rheumatol. 2011;7:33–42.
57. Müller-Ladner U, Pap T, Gay RE, Neidhart M, Gay S. Mechanisms of disease: the molecular and cellular basis of joint destruction in rheumatoid arthritis. Nat Rev Rheumatol. 2005;1:102–10.
58. Murphy G, Nagase H. Reappraising metalloproteinases in rheumatoid arthritis and osteoarthritis: destruction or repair? Nat Clin Pract Rheumatol. 2008;4:128–35.

Publisher's Note